Chaos, Solitons and Fractals 186 (2024) 115248

Contents lists available at ScienceDirect

Chaos, Solitons and Fractals

journal homepage: www.elsevier.com/locate/chaos

Homoclinic behavior around a degenerate heteroclinic cycle in a Lorenz-like system

A. Algaba [a,1], F. Fernández-Sánchez [b,1], M. Merino [a,1], A.J. Rodríguez-Luis [b,1,*]

[a] Departamento de Matemáticas, Centro de Investigación de Física Teórica y Matemática FIMAT, Universidad de Huelva, 21071 Huelva, Spain
[b] Departamento de Matemática Aplicada II & IMUS, E.T.S. Ingeniería, Universidad de Sevilla, Camino de los Descubrimientos s/n, 41092 Sevilla, Spain

ARTICLE INFO

Keywords:
Degenerate heteroclinic cycle
Lorenz-like system
Homoclinic connection
Belyakov degeneracy
Triple-zero bifurcation

ABSTRACT

In this work, we analyze a degenerate heteroclinic cycle that appears in a Lorenz-like system when one of the involved equilibria changes from real saddle to saddle-focus. First, from a theoretical model based on the construction of a Poincaré return map, we demonstrate that an infinite number of homoclinic connections arise from the point of the parameter plane where the degenerate heteroclinic cycle appears. The subsequent numerical study not only illustrates the presence of the first homoclinic orbits in the infinite succession but also allows to find other important local and global organizing centers of codimension two (Bogdanov–Takens bifurcations, degenerate homoclinic and heteroclinic connections, T-points) and three (triple-zero bifurcation, doubly-degenerate heteroclinic cycles, degenerate T-points).

1. Introduction

From the appearance of Lorenz system [1], it became clear that an autonomous three-dimensional system can exhibit very complex behaviors in certain regions of its parameter space. To illustrate this statement, and without intending to be exhaustive, we are going to cite some works on several systems widely studied in the literature (see also the references therein). Thus, some aspects of the chaotic behavior exhibited by the Lorenz system are analyzed in [2,3], and the detection of hidden chaotic attractors is reported in [4]. How and where preturbulence arises in its three-dimensional phase space is determined by the computation of global invariant manifolds [5]. The existence of invariant algebraic surfaces and their consequences on global dynamics are examined in [6]. In [7], the authors peruse the presence of resonances of periodic orbits in Lorenz system whereas in [8] the so-called superluminal periodic orbits (with unbounded amplitude and whose period tends to zero) are detected.

Regarding the paradigmatic Rössler system [9], resonances of periodic orbits in the vicinity of a triple-zero bifurcation are studied in [10], whereas a detailed qualitative and numerical analysis is presented in [11]. In the case of Chua's equation [12], a stability analysis is carried out in [13]. The presence of Shilnikov homoclinic connections [14] and other degenerate global bifurcations (for instance, Belyakov points [15,16] and T-point-Hopf [17]) helps to understand the complex dynamics that Chua's equation can exhibit. Other works have focused on the presence of chaotic behavior in some electronic circuits [18,19], brushless DC motors [20] and Lorenz-like systems [21]. The relationship between invariant tori and strange attractors has also been studied [22].

The combination of analytical and numerical techniques has been revealed as an effective procedure to obtain relevant information about the dynamics of these systems [23]. On the one hand, the detection and study of the possible local bifurcations of the equilibria (with the analysis of the corresponding normal forms) usually constitute a good starting point to determine the organizing centers of the dynamics [24–26]. An usual way to locate a global connection is by numerical continuation of a limit cycle born in a Hopf bifurcation (the Jacobian matrix has a pair of purely imaginary eigenvalues) [27]. On the other hand, it is well known that a Bogdanov–Takens bifurcation (a double-zero eigenvalue with geometric multiplicity one) guarantees the existence of global connections in their vicinity (a homoclinic orbit in the generic case and a pair of homoclinic or heteroclinic orbits in a symmetric system; recall that a homoclinic connection is bi-asymptotic to a saddle equilibrium whereas a heteroclinic connection joins two different saddle equilibria). Starting from this bifurcation, it has been possible to advance in the study of systems from very diverse fields, such as, for example, the Lorenz system [28], electronic circuits [29,30], control systems [31], ecological models [32,33] and epidemic models [34]. In the case in which the double-zero eigenvalue has geometric multiplicity two, it has recently been shown that heteroclinic connections appear for certain values of the parameters [35–37]. It is also known that the

* Corresponding author.
E-mail addresses: algaba@uhu.es (A. Algaba), fefesan@us.es (F. Fernández-Sánchez), merino@uhu.es (M. Merino), ajrluis@us.es (A.J. Rodríguez-Luis).
[1] All authors contributed equally to the present research work. All authors read and approved the final manuscript.

https://doi.org/10.1016/j.chaos.2024.115248
Received 17 May 2024; Received in revised form 1 July 2024; Accepted 4 July 2024
Available online 13 July 2024

presence of a Hopf-zero degeneration can lead to the presence of global connections [38,39]. It is also important to highlight that the triple-zero linear degeneracy is a major organizing center in many chaotic systems as, for instance, in optical laser models [40], in Rössler system [41] and in tritrophic food chains [42]. As we will see, this bifurcation also plays a crucial role in the system we study in this paper.

The primary works of Shilnikov revealed the complex dynamics that the presence of a homoclinic connection to a saddle-focus can entail, namely the existence of infinitely many saddle limit cycles in each neighborhood of the homoclinic orbit, the so-called "Shilnikov chaos" (see the recent survey [43] and references therein). Given the difficulty of obtaining analytical results on global connections (see, for instance, [44,45]), numerical methods are essential for completing their study (which implicates finding them, analyzing them, and continuing the loci in the parameter space in which they exist). Detecting degeneracies in global connections is a crucial task as it will allow us to find important changes in the nearby dynamics. Degenerate global connections appear when some non-degeneracy conditions (local and/or global) are violated (for instance, conditions on the eigenvalues of the equilibria involved or on the orientability of their stable and unstable manifolds). If one non-degeneracy condition is unfulfilled, a codimension-two global bifurcation occurs (and typically new bifurcation curves exist in a neighborhood of the corresponding point in the parameter plane) [46,47].

If we restrict ourselves to the case of heteroclinic connections between two equilibria, the presence of a heteroclinic cycle (a loop formed by two heteroclinic orbits) can lead to interesting dynamical consequences. In a generic system, a heteroclinic cycle corresponds to a bifurcation of codimension two. However, when the system has some symmetry, it can be of codimension one because two symmetric heteroclinic orbits form the cycle. In the case we are going to analyze (both theoretically and numerically) throughout this work, the two equilibria are connected not only by a pair of symmetric heteroclinic orbits, but also by another heteroclinic orbit of codimension zero (because it always exists). In other words, there are two heteroclinic cycles that share an orbit that is always present.

In this work, we will find some degenerate global connections that we will now briefly comment on, along with some appropriate references. Thus, a Belyakov degeneracy appears when the/an equilibrium involved in the global connection changes from real saddle to saddle-focus [48,49] (recall that, in planar systems, a saddle equilibrium has two eigenvalues of different signs; in three-dimensional systems, when the three eigenvalues are real, it is named *real saddle*, whereas if the equilibrium has a pair of complex conjugate eigenvalues, it is called *saddle-focus*). This degeneration, which entails the existence of extremely complex behaviors, has been found, for example, in Rössler system [50,51], in tritrophic food chain models [52], in electronic circuits [53] and in economic growth models [54]. In a Hopf-Shil'nikov degeneration, the corresponding equilibrium connected by a Shilnikov homoclinic orbit is no longer hyperbolic as it undergoes a Hopf bifurcation [55–57] (homoclinic tangencies to periodic orbits exist on the other side of the Hopf curve). In a three-dimensional system having at least two equilibria, a T-point (also called Bykov cycle [58]) occurs when the one-dimensional unstable manifold of one of the equilibria and the one-dimensional stable manifold of the other equilibrium match and, simultaneously, the two-dimensional manifolds of these equilibria have a transversal intersection, giving rise to a heteroclinic loop. This codimension-two bifurcation has been found, for instance, in the Lorenz system [59,60] (when the equilibrium at the origin is a real saddle and the nontrivial equilibria are saddle-foci) and in electronic circuits [61,62] (in this case all the equilibria are saddle-foci). The existence of repelling dynamics near a T-point has been proved in [63]. Finally, a homoclinic connection to a real saddle exhibits an inclination flip when the stable manifold of the equilibrium changes from orientable to nonorientable (Möbius band) and the eigenvalues satisfy certain conditions. There are three cases of a homoclinic flip bifurcation (named A, B, and C, in increasing order of complexity) [47,64,65].

This paper is organized as follows. In Section 2, we construct a theoretical model to study a degenerate heteroclinic cycle connecting two equilibria, one of which changes from real saddle to saddle-focus (Belyakov transition). The cycle is formed by two heteroclinic orbits. One of them is placed on an invariant axis, and consequently, it exists for all values of the parameters (codimension zero), and the other one is structurally unstable (codimension one). The model is based on the construction of a Poincaré return map. Its study allows us to demonstrate that an infinite number of homoclinic connections arise from the point on the parameter plane where the degenerate heteroclinic cycle appears. To the best of our knowledge, this result has not been proven so far in the literature.

In Section 3, we consider a Lorenz-like system that exhibits the above degenerate heteroclinic bifurcation. The numerical analysis we perform has two goals. On the one hand, to illustrate the validity of the previous theoretical analysis. On the other hand, to detect organizing centers of the dynamics of the system in a three-parameter space and connect them to each other. In this way, we will find several bifurcations of codimension three, both local (a triple-zero bifurcation) and global (doubly-degenerate heteroclinic cycles and degenerate T-points). The points corresponding to these bifurcations are connected by curves where codimension-two bifurcations occur, both local (two Bogdanov–Takens, a Hopf-zero, a double-zero) and global (a Hopf–Shilnikov heteroclinic cycle, a degenerate heteroclinic cycle, degenerate homoclinic connections, T-points). We end this paper with Section 4, Conclusions and future works.

2. Analysis of a degenerate heteroclinic cycle

This section is devoted to giving an analytical explanation of the appearance of homoclinic connections in the neighborhood of a global cycle that connects a real saddle equilibrium with a saddle-degenerate node for some values of the parameters under a particular symmetry (as we detail below, the saddle-degenerate node that we consider has a double positive eigenvalue, in such a way that when moving a parameter, this equilibrium changes from real saddle to saddle-focus). More concretely, let us consider, for every $\mathbf{x} = (x_1, x_2, x_3)$ in $\mathbb{R}^3$ and every value of the pair of principal parameters $M = (M_1, M_2)$ in a neighborhood V of $0 \in \mathbb{R}^2$, a generic two-parameter family $\dot{\mathbf{x}} = X(\mathbf{x}; M)$ which satisfies the following hypotheses:

Hypothesis 1. The family is invariant under the involution $S(x_1, x_2, x_3) = (-x_1, -x_2, x_3)$ for every value of parameter $M \in V$.

Therefore, the straight line given by

$$Fix(S) = \left\{(x_1, x_2, x_3) \in \mathbb{R}^3 : x_1 = 0, x_2 = 0\right\},$$

that is, the x_3-axis, is invariant for the flow of every system of the family.

Hypothesis 2. For every $M \in V$, the family has just two equilibria Q_1 and Q_2 located at $Fix(S)$, such that the eigenvalues of their respective linearization matrices $\left(\mu_1(M), \mu_2(M), \mu_3(M)\right)$ and $\left(\lambda_1(M), \lambda_2(M), \lambda_3(M)\right)$ are smooth functions of M such that for $M = 0$ are given by

$$\left(\mu_1(0), \mu_2(0), \mu_3(0)\right) = \left(P_0, P_0, -\Lambda_0\right)$$

where $P_0, \Lambda_0 > 0$ and

$$\left(\lambda_1(0), \lambda_2(0), \lambda_3(0)\right) = \left(-\lambda_{10}, \lambda_{20}, \lambda_{30}\right)$$

where $\lambda_{20} > \lambda_{30} > 0$ and $\lambda_{10} > 0$.

As long as it is not necessary, from now on, we will get rid of the M argument when we use these or other parameters.

As a first consequence of Hypotheses 1 and 2, both equilibria Q_1 and Q_2 are always connected, for all the values of the parameter $M \in V$,

by a heteroclinic orbit $\Gamma_1 \subset r$. In fact, this orbit is included in the stable one-dimensional manifold $W^s_{Q_1}$ and in the two-dimensional unstable manifold $W^u_{Q_2}$ and, generically, it corresponds to the one-dimensional leading unstable manifold $W^{lu}_{Q_2}$ given by the eigenspace of eigenvalue λ_3. See Fig. 1(a) for a sketch of Γ_1.

Due to the symmetry, Γ_1 is invariant for all the values of $M \in V$ and therefore, its codimension is zero.

Hypothesis 3. For $M = 0$ there exists a generic heteroclinic connection Γ_2 joining Q_1 and Q_2, involving manifolds $W^u_{Q_1}$ and $W^s_{Q_2}$.

Remark that $W^u_{Q_1}$ is two-dimensional whereas $W^s_{Q_2}$ is one-dimensional. See Fig. 1(a) for a sketch of Γ_2 and the complete cycle.

Under Hypothesis 2, it is well known (see, for instance, [52]) that after a suitable change of variables and time, in a neighborhood of Q_1 and the critical parameter $M = 0$, any generic system satisfying this hypothesis can be written, in new coordinates (X, Y, Z), as

$$\begin{cases} \dot{X} = P(M)\,X + Y + F_{1,1}(X,Y,Z,M)\,X + F_{1,2}(X,Y,Z,M)\,Y, \\ \dot{Y} = -M_1 X + P(M)\,Y + F_{2,1}(X,Y,Z,M)\,X + F_{2,2}(X,Y,Z,M)\,Y, \\ \dot{Z} = -\Lambda(M)\,Z, \end{cases} \tag{1}$$

where the smooth functions P and Λ verify $P(0) = P_0 > 0$ and $\Lambda(0) = \Lambda_0 > 0$, while $F_{i,j}$, for each pair $i, j = 1, 2$, are smooth functions of their arguments. For $M_1 = 0$ the equilibrium Q_1 is a degenerate saddle, for $M_1 < 0$ it is a real saddle (whose eigenvalues are real and simple), while for $M_1 > 0$ it is a saddle-focus (a pair of complex eigenvalues with positive real part and a negative eigenvalue).

Now that the role of the principal parameter M_1 (as the one that controls the transition from node to focus) has been established and since, without lack of generality, the principal parameters M_1 and M_2 can be chosen to be independent of each other, it is a good time to determine the effect of changing the values of the second principal parameter M_2 on the flow of the system. To this end, we must take into account that, although we have assumed in hypothesis (H3) that $W^s_{Q_2}$ and $W^u_{Q_1}$ intersect for $M = 0$, the genericity of the corresponding heteroclinic connection implies that these manifolds cannot intersect for every small M. Therefore, the parameter M_2 should be selected to control the relative position between $W^s_{Q_2}$ and $W^u_{Q_1}$ in such a way that for every M with $M_2 = 0$ and $\|M\|$ small, they have a transversal intersection and, consequently, a generic heteroclinic orbit.

With the choice of the coordinates (X, Y, Z) for system (1), the one-dimensional invariant stable manifold $W^s_{Q_1}$ coincides with the Z-axis (that corresponds with the previous x_3-axis). Analogously, the two-dimensional invariant unstable manifold $W^u_{Q_1}$ locally coincides with the plane $Z = 0$.

Regarding the other equilibrium, by a smooth change of variables in a neighborhood of Q_2 and when $\|M\|$ is small, it is possible to choose coordinates (x, y, z) such that the one-dimensional invariant stable manifold $W^s_{Q_2}$ corresponds to the x-axis and the two-dimensional invariant unstable manifold $W^u_{Q_2}$ locally coincides with the plane $x = 0$ (see, for instance, [66]). Moreover, this change may be chosen in such a way that the z-axis corresponds with the previous x_3-axis.

In this work, we are interested in the study of the homoclinic orbits to Q_2 that appear from the global heteroclinic cycle $Q_1 \cup \Gamma_1 \cup Q_2 \cup \Gamma_2$ when $\|M\|$ is small with $M_1 \geq 0$. The technique used, as usual in many other papers (see, for instance, [52,67]), is based on the construction of a Poincaré return map in a neighborhood of the heteroclinic cycle, via the choice of four suitable transversal planar sections in order to divide the flow in two local regions around each equilibrium and two global transitions between them.

Since the heteroclinic orbits Γ_1, for every $M \in V$, and Γ_2, for $M = 0$, locally correspond, in a neighborhood of Q_2, with the x and z axes, we take sections

$$\Sigma_1 = \{(x, y, z) : \ x = h_x\},$$

where h_x is a small positive value and y, z are small, and

$$\Sigma_2 = \{(x, y, z) : \ z = h_z\},$$

for a small $h_z > 0$, $x > 0$, and y. Note that these sections could also be used for symmetric orbits with the change $(x, y) \leftrightarrow (-x, -y)$.

Near Q_1, since the orbit Γ_1 corresponds to the Z-axis for every $M \in V$, we take section

$$\Sigma_3 = \{(X, Y, Z) : \ Z = H\},$$

where $H > 0$ and X, Y are small.

Finally, let us call Y_0 the Y coordinate of the intersection between Γ_2 and the plane $X = 0$ close to Q_1 for $M = 0$. Therefore, we take

$$\Sigma_4 = \{(X, Y, Z) : \ X = 0\},$$

where Z and Y belong to a small disc of Σ_4 around the point $(0, Y_0, 0)$. As above, the change $(X, Y) \leftrightarrow (-X, -Y)$ allows to study the symmetric orbits.

Since this analysis is focused on the set of homoclinic connections of equilibrium Q_2, in order to make easier and simpler some reasonings and expressions, it is convenient to define all the needed transitions in the opposite direction of flow. That is, T_{14} from Σ_1 to Σ_4, T_{43} from Σ_4 to Σ_3, and T_{32} from Σ_3 to Σ_2. Note that, beyond the local characterization of $W^s_{Q_2}$ as the x-axis and $W^u_{Q_2}$ as the plane $x = 0$, an explicit expression for the local map between Σ_1 and Σ_2 is not necessary for these homoclinic connections to Q_2.

The local map $T_{43} : \Sigma_4 \to \Sigma_3$ is obtained by direct integration of system (1) (see, for instance, [52,68]), that is, $T_{43}(0, Y, Z) = (\bar{X}, \bar{Y}, H)$ for

$$\begin{bmatrix} \bar{X} \\ \bar{Y} \end{bmatrix} = \begin{bmatrix} \dfrac{1}{\sqrt{M_1}} Y Z^{\Delta} H^{-\Delta} \sin\left(\dfrac{\sqrt{M_1}}{\Lambda} \log\left(\dfrac{Z}{H}\right)\right) + o\left(Z^{\Delta}\right) \\ Y Z^{\Delta} H^{-\Delta} \cos\left(\dfrac{\sqrt{M_1}}{\Lambda} \log\left(\dfrac{Z}{H}\right)\right) + o\left(Z^{\Delta}\right) \end{bmatrix}, \tag{2}$$

where

$$\Delta = \frac{P}{\Lambda} > 0, \tag{3}$$

for $\|M\|$ small. Note that, in order to simplify the expressions, we have removed the explicit dependence on M in Eqs. (2) and (3).

Due to its smoothness, the map $T_{32} : \Sigma_3 \to \Sigma_2$ can be written as $T_{32}(\bar{X}, \bar{Y}, H) = (x, y, h_z)$ for

$$\begin{bmatrix} x \\ y \end{bmatrix} = \begin{bmatrix} A & B \\ C & D \end{bmatrix} \begin{bmatrix} \bar{X} \\ \bar{Y} \end{bmatrix} + \begin{bmatrix} O(\bar{X}^2 + \bar{Y}^2) \\ O(\bar{X}^2 + \bar{Y}^2) \end{bmatrix}, \tag{4}$$

where A, B, C, and D are smooth functions on M such that $A(0)D(0) - B(0)C(0) \neq 0$. Without loss of generality, it can also be assumed that $\|M\|$ is small enough to ensure $AD - BC \neq 0$ for every M.

We can also assume that $A(0) \neq 0$ and so $A \neq 0$ for small $\|M\|$. Note that $A(0) = 0$ corresponds to the non-generic scenario in which the straight line $\bar{Y} = 0$ in Σ_3 (that is, the eigenspace associated to the repeated eigenvalue P_0) is mapped onto $x = 0$ in Σ_2 (that is, the two-dimensional unstable manifold $W^u_{Q_2}$).

In the other global map $T_{14} : \Sigma_1 \to \Sigma_4$, the other parameter M_2 appears explicitly to control the relative position between $W^s_{Q_2}$ and the two-dimensional manifold $W^u_{Q_1}$ (that locally coincides with $Z = 0$). See, for instance, [52]. Therefore, $T_{14}(h_x, \bar{y}, \bar{z}) = (0, Y, Z)$, where

$$\begin{bmatrix} Y \\ Z \end{bmatrix} = \begin{bmatrix} Y_0 \\ M_2 \end{bmatrix} + \begin{bmatrix} a & b \\ c & d \end{bmatrix} \begin{bmatrix} \bar{y} \\ \bar{z} \end{bmatrix} + \begin{bmatrix} O(\bar{y}^2 + \bar{z}^2) \\ O(\bar{y}^2 + \bar{z}^2) \end{bmatrix}, \tag{5}$$

where a, b, c, and d are smooth functions on M such that $a(0)d(0) - b(0)c(0) \neq 0$. Without loss of generality, it can also be assumed that $\|M\|$ is small enough to ensure $ad - bc \neq 0$ for every M. Moreover, we assume $M_2 > 0$ to ensure the reinjection of $W^s_{Q_2}$ in the $Z > 0$ half of Σ_4.

Once the needed maps have been determined, let us impose the conditions that a homoclinic connection to Q_2 must satisfy. First of all,

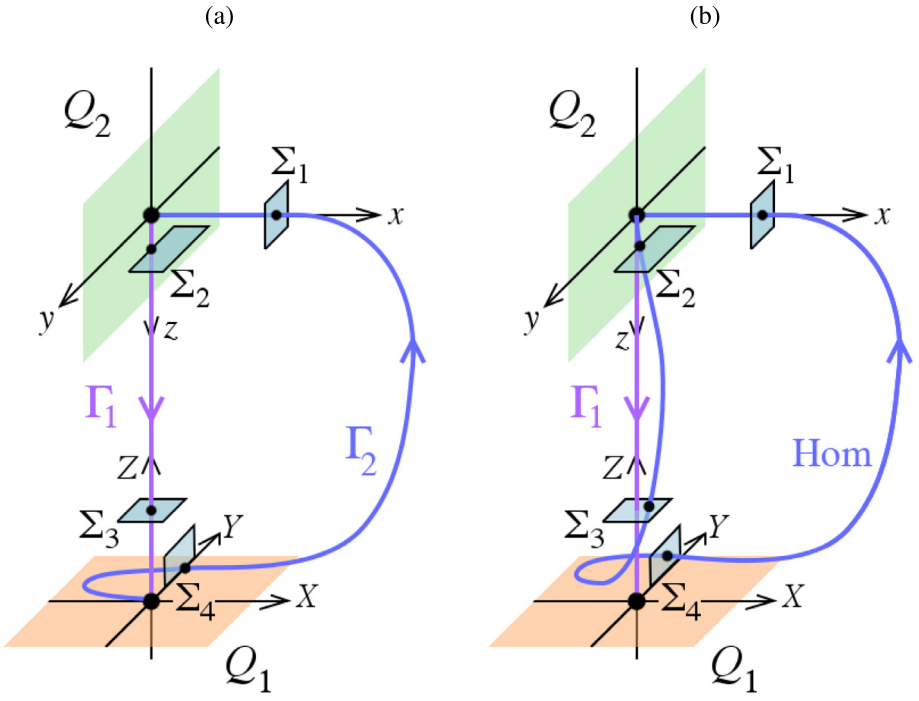

Fig. 1. (a) Schematic drawing of the global heteroclinic cycle $Q_1 \cup \Gamma_1 \cup Q_2 \cup \Gamma_2$ for $M = 0$. (b) Schematic drawing for $M_1 > 0$ of a homoclinic connection to Q_2 close to the heteroclinic cycle. The heteroclinic orbit Γ_1 that goes from Q_2 to Q_1 in positive time, is invariant to the flow for every value $M \in V$.

the point $(h_x, 0, 0) \in \Sigma_1$, that corresponds to $W^s_{Q_2}$, is mapped by T_{14} to the point $(0, Y_0, M_2) \in \Sigma_4$. Now, this point is mapped by T_{43} to $(\bar{X}, \bar{Y}, H)$ where

$$\begin{bmatrix} \bar{X} \\ \bar{Y} \end{bmatrix} = \begin{bmatrix} \frac{1}{\sqrt{M_1}} Y_0 M_2^{\Delta} H^{-\Delta} \sin\left(\frac{\sqrt{M_1}}{\Lambda} \log\left(\frac{M_2}{H}\right)\right) + o\left(M_2^{\Delta}\right) \\ Y_0 M_2^{\Delta} H^{-\Delta} \cos\left(\frac{\sqrt{M_1}}{\Lambda} \log\left(\frac{M_2}{H}\right)\right) + o\left(M_2^{\Delta}\right) \end{bmatrix}.$$

Finally, in order to have a homoclinic connection to Q_2, this point $(\bar{X}, \bar{Y}, H)$ must be mapped by T_{32} to a point $(0, y, h_z) \in \Sigma_2$. This implies that

$$0 = Y_0 M_2^{\Delta} H^{-\Delta} \left(\frac{A}{\sqrt{M_1}} \sin\left(\frac{\sqrt{M_1}}{\Lambda} \log\left(\frac{M_2}{H}\right)\right) + B \cos\left(\frac{\sqrt{M_1}}{\Lambda} \log\left(\frac{M_2}{H}\right)\right)\right) + o\left(M_2^{\Delta}\right).$$

Since A does not vanish for $\|M\|$ small, this implies that

$$\sin\left(\frac{\sqrt{M_1}}{\Lambda} \log\left(\frac{M_2}{H}\right)\right) = \sqrt{M_1}\, \Phi(M), \tag{6}$$

where Φ is bounded for $\|M\|$ small. Therefore, it is obvious that for every M_1 small, this equation has infinitely many solutions M_2. This fact is illustrated in Fig. 2(a).

Moreover, if we write

$$\frac{\sqrt{M_1}}{\Lambda} \log\left(\frac{M_2}{H}\right) = -n\pi + \theta,$$

where $n \in \mathbb{N}$ is sufficiently big and $\theta \in [-\pi/2, \pi/2)$, we have $\sin(\theta) = (-1)^n \sqrt{M_1}\, \Phi(M)$ and so $\theta = O\left(\sqrt{M_1}\right)$ for $\|M\|$ small.

Finally, solving (6) for M_2, the following first-order approach is obtained for the curves of homoclinic connections to Q_2 in the space of parameters,

$$M_2 = H \exp\left(\frac{\Lambda\left(-n\pi + O\left(\sqrt{M_1}\right)\right)}{\sqrt{M_1}}\right).$$

This expression leads to the arrangement of the homoclinic curves schematized in Fig. 2(b).

The above reasonings can be summarized in the following theorem:

Theorem 2.1. *Let us consider, for every $\mathbf{x} = (x_1, x_2, x_3)$ in $\mathbb{R}^3$ and every $M = (M_1, M_2)$ in a neighborhood V of $0 \in \mathbb{R}^2$, a generic two-parameter family $\dot{\mathbf{x}} = X(\mathbf{x}; M)$ which satisfies the Hypotheses 1, 2, and 3. Then, from the origin of the (M_1, M_2)-parameter plane, (countable) infinitely many curves of homoclinic connections to Q_2 emerge.*

We finish this section with an important remark. It is well known that homoclinic bifurcations involving a real saddle to saddle-focus transition (Belyakov point; see, for instance, [48,49,52]) give rise to the appearance of (countable) infinitely many curves of homoclinic connections to the saddle-focus equilibrium in the parameter plane. What is noteworthy here is that the infinitely many curves of homoclinic connections given by the theorem correspond to the equilibrium Q_2, which does not exhibit this transition.

3. Numerical study

Next, we consider a Lorenz-like system that will illustrate the theoretical results stated in the previous section. Specifically, we will numerically find the first five elements of the predicted sequence of infinitely many homoclinic orbits. This numerical study will also allow us to find other important organizing centers of the complex dynamics exhibited by the system that we are going to analyze, namely

$$\begin{cases} \dot{x} = y, \\ \dot{y} = a_1 x + a_2 y + Axz + Byz, \\ \dot{z} = a_3 z + Cx^2 + Dz^2, \end{cases} \tag{7}$$

where $a_1, a_2, a_3 \in \mathbb{R}$ and A, B, C, D are real parameters. This system encompasses others widely studied in the literature. If $A = -1$, $C = 1$, $B = D = 0$, we obtain as particular cases the Shimizu-Morioka system [69,70] and a laser model [71] (for $a_1 = 1, a_2 = -\lambda, a_3 = -\alpha$) and a low-order model of magnetoconvection [72] (for $a_1 = -\lambda, a_2 = k, a_3 = -1$). When $A = -a\,k, C = h, B = D = 0$, a Lorenz-like system is

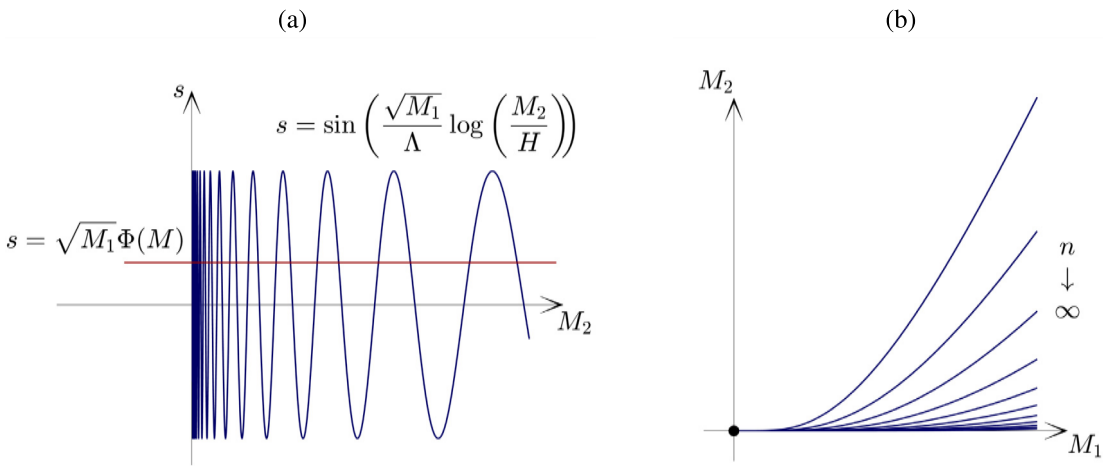

Fig. 2. (a) For a fixed small value of M_1, a schematic drawing of the infinite solutions of Eq. (6) when M_2 tends to 0. (b) Curves of homoclinic connections to Q_2 in a neighborhood of the origin in the first quadrant of the (M_1, M_2)-parameter plane. The origin corresponds to the heteroclinic cycle that involves the degenerate real saddle equilibrium Q_1, as shown in Fig. 1(a).

obtained [73,74] (for $a_1 = a\,b, a_2 = -a, a_3 = -c$), using the change of variables $x = \widetilde{x}, y = a(\widetilde{y}-\widetilde{x}), z = \widetilde{z}$. Furthermore, for $a_1, a_2, a_3 \approx 0$, system (7) corresponds to a three-parametric unfolding of a normal form for the triple-zero bifurcation in the Lorenz system [35,75].

If $AC \neq 0$, with an appropriate scaling, we can take $A = C = 1$. Thus, from now on, we study the system

$$\begin{cases} \dot{x} = y, \\ \dot{y} = a_1 x + a_2 y + xz + Byz, \\ \dot{z} = a_3 z + x^2 + Dz^2. \end{cases} \tag{8}$$

Its equilibria are the origin $E_1 = (0,0,0)$, $E_2 = (0,0,-a_3/D)$ if $a_3, D \neq 0$ and, when $a_1(a_3 - Da_1) > 0$, a pair of symmetric equilibria $E_{3,4} = (\pm\sqrt{a_1(a_3 - Da_1)}, 0, -a_1)$. We remark that the equilibria E_1 and E_2 are located on the z-axis, which is an invariant set because the system is invariant under the change $(x, y, z) \to (-x, -y, z)$.

We make two comments about the notation that we will use throughout this paper so that it does not become too complicated. First, although a global bifurcation (homoclinic or heteroclinic) appearing in parameter space and the corresponding orbit in phase space are two different objects, we will assign the same label when referring to them (since there is no possibility of confusion). Secondly, when necessary, we will add a superscript to the label of a bifurcation in order to specify the equilibrium involved.

The characteristic polynomial of the linearization matrix of system (8) at the origin is $p = \lambda^3 + p_1\lambda^2 + p_2\lambda + p_3$, where

$$p_1 = -(a_2 + a_3), \quad p_2 = a_2 a_3 - a_1, \quad p_3 = a_1 a_3.$$

Consequently, it is guaranteed that the origin E_1 undergoes, among others, the next bifurcations:

- a pitchfork bifurcation $\mathbf{P^1}$ when $p_3 = 0, p_1 \neq 0 \neq p_2$, i.e., for $a_1 = 0$, $a_2 \neq 0 \neq a_3$. Two new equilibria $E_{3,4}$ appear when $a_1(a_3 - Da_1) > 0$.
- a Hopf bifurcation $\mathbf{h^1}$ if $p_1 p_2 = p_3$, $p_2 > 0$, $p_1 \neq 0$, that is, for $a_2 = 0$, $a_1 < 0$, $a_3 \neq 0$.
- a Bogdanov–Takens bifurcation $\mathbf{BT^1}$ when $p_2 = p_3 = 0$, $p_1 \neq 0$, i.e., for $a_1 = a_2 = 0$, $a_3 \neq 0$. We study now this bifurcation.
  The eigenvalues of the linearization matrix at the origin are $\lambda_{1,2} = 0$ and $\lambda_3 = a_3 \neq 0$. Therefore, it has a local invariant manifold of codimension one $\mathcal{W}^c$ (center manifold; see, for instance, [23]) which in local coordinates is given by $z = h(x, y)$, where h is a smooth function in a neighborhood of the origin. Imposing $z = h(x, y)$ to be an invariant manifold of (8) at the critical values, $a_1 = a_2 = 0$, $a_3 \neq 0$, we obtain

$$z = -\frac{1}{a_3}x^2 - \frac{2}{a_3^2}xy - \frac{2}{a_3^3}y^2 + \mathcal{O}\left(|x, y|^3\right).$$

Consequently, the dynamics on the center manifold is given by the reduced two-dimensional system

$$\begin{cases} \dot{x} = y, \\ \dot{y} = -\frac{1}{a_3}x^3 - \left(\frac{2}{a_3^2} + \frac{B}{a_3}\right)x^2 y - \left(\frac{2}{a_3^3} + \frac{2B}{a_3^2}\right)xy^2 \\ \qquad - \frac{2B}{a_3^3}y^3 + \mathcal{O}\left(|x, y|^4\right). \end{cases}$$

Thus, the reduced system up to order three in normal form (see [23]) is

$$\begin{cases} \dot{x} = y, \\ \dot{y} = -\frac{1}{a_3}x^3 - \left(\frac{2}{a_3^2} + \frac{B}{a_3}\right)x^2 y. \end{cases} \tag{9}$$

Since $\frac{1}{a_3} \neq 0$ and $\frac{2}{a_3^2} + \frac{B}{a_3} \neq 0$, this truncated normal form captures all the dynamics of the Bogdanov–Takens bifurcation in a neighborhood of the equilibrium, for a vicinity of the parameters close to the critical values, $a_1 \approx 0$, $a_2 \approx 0$, $a_3 \neq 0$. Scaling the state variables and the time we have

$$\begin{cases} X' = Y, \\ Y' = -\text{sign}(a_3)X^3 - X^2 Y. \end{cases} \tag{10}$$

Therefore, the Bogdanov–Takens bifurcation of E_1 is of homoclinic type if $a_3 > 0$ and of heteroclinic type when $a_3 < 0$ (see [23] and also the other classical textbooks [24–26]).

Note that the origin also exhibits transcritical (when $a_3 = 0$, $a_1, a_2, D \neq 0$), Hopf-zero (if $a_2 = a_3 = 0$, $a_1 < 0$), double-zero (for $a_1 = a_3 = 0$, $a_2 \neq 0$; a double-zero eigenvalue with geometrical multiplicity two), and triple-zero (if $a_1 = a_2 = a_3 = 0$; a triple-zero eigenvalue with geometrical multiplicity two) bifurcations [35]. These last three will appear at the end of the work when we draw a partial bifurcation set in the (a_1, a_2, a_3)-parameter space (see Figs. 10(a)–(d)).

The bifurcations of $E_2 = (0, 0, \frac{-a_3}{D})$ can be easily calculated. To do so we translate it to the origin by means of the change

$$x = X, \ y = Y, \ z = Z - \frac{a_3}{D},$$

that transforms system (8) into

$$\begin{cases} \dot{X} = Y, \\ \dot{Y} = (a_1 - \frac{1}{D}a_3)X + (a_2 - \frac{B}{D}a_3)Y + XZ + BYZ, \\ \dot{Z} = -a_3 Z + X^2 + DZ^2, \end{cases} \tag{11}$$

with $a_3, D \neq 0$.

Comparing systems (8) and (11) we deduce that (8) is symmetric to the change

$$(x, y, z, t, a_1, a_2, a_3, B, D) \longrightarrow \left(x, y, z - \frac{a_3}{D}, t, a_1^*, a_2^*, a_3^*, B, D\right), \tag{12}$$

where

$$a_1^* = a_1 - \frac{1}{D}a_3, \quad a_2^* = a_2 - \frac{B}{D}a_3, \quad a_3^* = -a_3.$$

According to this, it is very easy to obtain the bifurcations of the equilibrium E_2 by transferring those of E_1. Thus, E_2 exhibits:

- a pitchfork bifurcation **P²** when $a_1^* = 0$, $a_2^* \neq 0 \neq a_3^*$, i.e., for $a_1 = \frac{1}{D}a_3$, $a_2 \neq \frac{B}{D}a_3$, $a_3 \neq 0$. Two new equilibria $E_{3,4}$ appear when $a_1(a_3 - Da_1) > 0$.
- a Hopf bifurcation **h²** if $a_2^* = 0$, $a_1^* < 0$, $a_3^* \neq 0$, that is, when $a_2 = \frac{B}{D}a_3$, $a_1 < \frac{1}{D}a_3$, $a_3 \neq 0$.
- a Bogdanov–Takens bifurcation **BT²** when $a_1^* = a_2^* = 0$, $a_3^* \neq 0$, i.e., for $a_1 = \frac{1}{D}a_3$, $a_2 = \frac{B}{D}a_3$, $a_3 \neq 0$. It is of homoclinic type if $a_3 < 0$ and of heteroclinic type when $a_3 > 0$.

Our first objective is to study the heteroclinic loop between the equilibria E_1 and E_2 when one of them changes from real saddle to saddle-focus (degeneration that is usually called Belyakov point [48,49]) and then, check that the numerical results agree with the above theoretical analysis (specifically, showing that infinitely many homoclinic orbits arise from this degenerate point).

We are going to perform a numerical study with the help of the continuation code AUTO [76], of the bifurcation sets obtained in the vicinity of the Bogdanov–Takens bifurcation of the equilibrium E_2. To do this, we will fix $B = 0.2$ and $D = 1$ and then we will take slices $a_3 = constant$ in the (a_1, a_2, a_3)-parameter space. Note that, according to (12), to obtain the bifurcation set of system (8) it would be enough to do it for $a_3 < 0$, for example, and then translate all these solutions, through the aforementioned change, to the half-space $a_3 > 0$.

3.1. Study when $a_3 = -0.05$

First, we fix $a_3 = -0.05$. In this case, a Bogdanov–Takens bifurcation **BT²** (of homoclinic type) of the equilibrium E_2 occurs at the point $(a_1, a_2) = (-0.05, -0.01)$. The curves **P²** (given by $a_1 = -0.05$, $a_2 \neq -0.01$, where E_2 exhibits a pitchfork bifurcation) and **h²** (given by $a_2 = -0.01, a_1 < -0.05$, where E_2 experiments a Hopf bifurcation) emerge from **BT²**. Also, E_1 exhibits a Bogdanov–Takens bifurcation **BT¹** (of heteroclinic type), at the point $(a_1, a_2) = (0, 0)$. This equilibrium undergoes a pitchfork bifurcation **P¹** (when $a_1 = 0$, $a_2 \neq 0$) and a Hopf bifurcation **h¹** (for $a_2 = 0, a_1 < 0$). In Fig. 3 we represent all these bifurcation points and curves. For the values of the parameters that we have set, and according to the condition $a_1(a_3 - Da_1) > 0$ for the existence of $E_{3,4}$, we deduce that these equilibria exist in the region between lines **P¹** and **P²**.

In order to numerically obtain the remaining bifurcation curves that arise from the point **BT²** (corresponding to a Hopf of the equilibria $E_{3,4}$, a homoclinic connection to E_2 and a saddle–node of large-amplitude periodic orbits [23–26]), we are going to draw several bifurcation diagrams. Firstly, we set $a_2 = 0.05$ and continue the equilibrium E_3 in the parameter a_1 (recall throughout this work that, because of the symmetry system (8) has, E_4 will exhibit the same bifurcations as E_3). We obtain that for $a_1 \approx -0.047109$ it experiences a Hopf bifurcation, which we will denote by **h**. The bifurcation diagram corresponding to the pair of small-amplitude repulsive asymmetric periodic orbits emerged from **h** is drawn in Fig. 4(a). It ends in a homoclinic bifurcation **H₁** of E_2 that exists when $a_1 \approx -0.046425$. The large-amplitude unstable symmetric periodic orbit emerged from the homoclinic bifurcation **H₁** exhibits two symmetry-breaking bifurcations **PPO**, when $a_1 \approx -0.0451038$ and $a_1 \approx -0.0190131$. This periodic orbit becomes a saddle at the first bifurcation and changes to unstable again after the second. For $a_1 \approx -0.0189845$, it undergoes a saddle–node bifurcation **SN** where it becomes again a saddle until it disappears into a new homoclinic bifurcation of E_2, **H₂**, when $a_1 \approx -0.0419303$. The projection onto the (x, z)-plane of the corresponding homoclinic orbits is represented in the inside of Fig. 4(a).

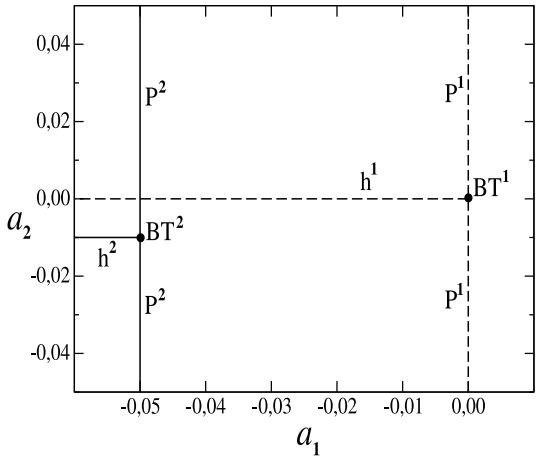

Fig. 3. For $B = 0.2$, $D = 1$, $a_3 = -0.05$, partial bifurcation set in a neighborhood of the points **BT¹** and **BT²**. The curves of the bifurcations exhibited by E_2 appear as solid lines and those related to E_1 as dashed lines.

Next, if we increase the value of the parameter to $a_2 = 0.5$, we obtain the bifurcation diagram in Fig. 4(b). Now, the repulsive small-amplitude asymmetric periodic orbit emerged from **h** ends in a heteroclinic bifurcation **He** between the real saddles $E_1 = (0, 0, 0)$ and $E_2 = (0, 0, 0.05)$, when $a_1 \approx -0.026142$. The heteroclinic loop is constituted by two heteroclinic orbits (see the inside of Fig. 4(b)). One is placed on the invariant z-axis (it exists for any value of the parameters) and the other one is placed outside this axis (it is structurally unstable).

Now we can numerically compute for $a_3 = -0.05$ the loci where some of the bifurcations detected in Fig. 4 occur in the (a_1, a_2)-plane. Thus, in Fig. 5 we show the curves **h** (Hopf bifurcation of the equilibria $E_{3,4}$), **H₁** (homoclinic connection to E_2) and **He** (heteroclinic cycle between E_1 and E_2).

The Hopf bifurcation curve **h**, emerged from **BT²**, is unbounded and asymptotic to the line $a_1 = \frac{a_3}{2D} = -0.025$ (as can be easily found). For its part, the curve **H₁** of homoclinic connections of E_2 arises from **BT²** and ends at the point **D₃He**, for $(a_1, a_2) \approx (-0.027249, 0.330145)$, located on the curve of heteroclinic connections **He**. This heteroclinic curve arises from the Hopf–Shil'nikov point **HS** (see, for instance, [55–57]), for $(-0.048818, 0)$, located on the curve $a_2 = 0$ where the equilibrium E_1 undergoes a Hopf bifurcation.

Due to the symmetry of system (8), a curve of saddle–node bifurcations of symmetric periodic orbits **SN** also arises from the point **BT²** [23,25,26], as can be seen in the inset of Fig. 5. This curve ends at a cusp bifurcation **CU**, for $(a_1, a_2) \approx (-0.0493143, 0.00261211)$, where it collapses with another saddle–node curve **SN** emerged from a degeneracy on the Hopf curve **h¹** (the first Lyapunov coefficient vanishes) which occurs when $(a_1, a_2) \approx (-0.0621875, 0)$, a point that is outside the range of the figure. Remark that, at a cusp bifurcation point, two saddle–node bifurcation curves meet tangentially. For nearby parameter values, the system can have three periodic orbits that collide and disappear pairwise via the two saddle–node bifurcations involved.

In the range of Fig. 5, the curve **h** does not present any degeneration (a pair of asymmetric repulsive periodic orbits arises to its right). In contrast, on the curve **H₁** a degeneracy occurs at the point **DH₁**, when $(a_1, a_2) \approx (-0.0415711, 0.108578)$. For their description, we denote the eigenvalues of the equilibrium E_2 by $\lambda_1^* < 0$, $0 < \lambda_2^*, \lambda_3^*$ (in the range of the above figure), and consider the saddle quantity $\delta_{E_2} = \left|\frac{min(\lambda_2^*, \lambda_3^*)}{\lambda_1^*}\right|$ where

$$\lambda_3^* = -a_3 = 0.05 > 0, \qquad \lambda_{2,1}^* = \frac{a_2 - 0.2a_3 \pm \sqrt{(a_2 - 0.2a_3)^2 + 4(a_1 - a_3)}}{2}.$$

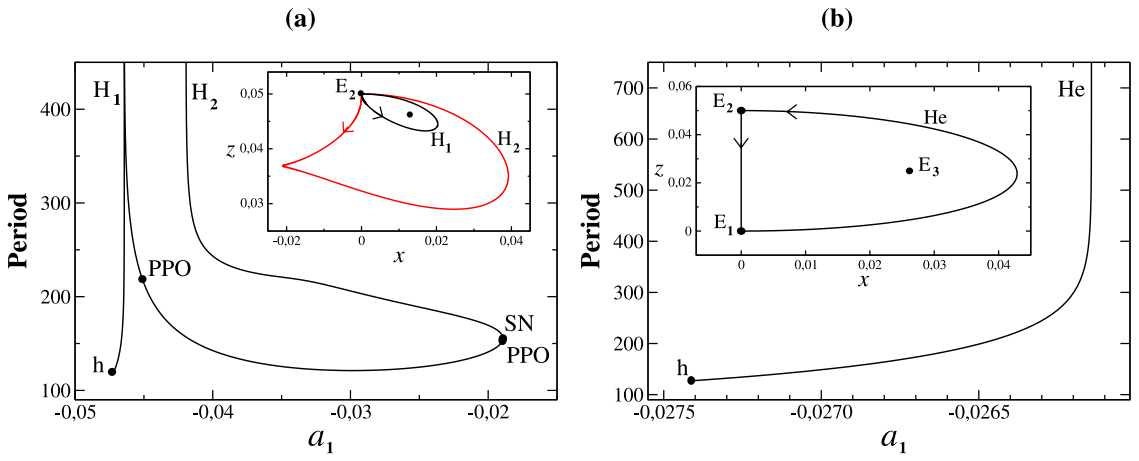

Fig. 4. For $B = 0.2$, $D = 1$, $a_3 = -0.05$: (a) Bifurcation diagram, when $a_2 = 0.05$, of small-amplitude asymmetric periodic orbits (which exist between the Hopf bifurcation **h** of E_3 and the homoclinic bifurcation $\mathbf{H_1}$ of E_2) and large-amplitude symmetric periodic orbits (which exist between the homoclinic bifurcations $\mathbf{H_1}$ and $\mathbf{H_2}$ of E_2). Projection onto the (x, z)-plane of the homoclinic connections $\mathbf{H_1}$ (black) and $\mathbf{H_2}$ (red) which exist, respectively, for $a_1 \approx -0.046425$ and $a_1 \approx -0.0419303$. (b) Bifurcation diagram, when $a_2 = 0.5$, of the small-amplitude asymmetric periodic orbits born in the Hopf bifurcation **h**, which disappear in the heteroclinic bifurcation **He**. Projection onto the (x, z)-plane of the corresponding heteroclinic cycle between E_1 and E_2, which appears for $a_1 \approx -0.026142$. (For interpretation of the references to color in this figure legend, the reader is referred to the web version of this article.)

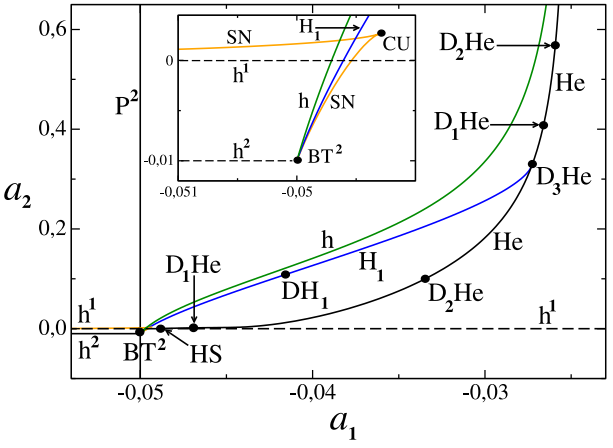

Fig. 5. For $B = 0.2$, $D = 1$, $a_3 = -0.05$, partial bifurcation set in a neighborhood of the point $\mathbf{BT^2}$.

When the curve $\mathbf{H_1}$ emerges from $\mathbf{BT^2}$, the equilibrium E_2 is a real saddle with $\delta_{E_2} > 1$ and a single symmetric repulsive periodic orbit emerges from the curve $\mathbf{H_1}$ towards the right and a pair of asymmetric repulsive periodic orbits exists on the left side of $\mathbf{H_1}$. The degeneracy $\mathbf{DH_1}$ is exhibited when $-\lambda_1^* = \lambda_3^* = 0.05$ because then $\delta_{E_2} = 1$ (resonant eigenvalues, see [46,47]). This degeneracy condition holds, when $a_3 = -0.05$, on the line $a_2 = 20a_1 + 0.94$.

From $\mathbf{DH_1}$, and to the point $\mathbf{D_3He}$ where the curve $\mathbf{H_1}$ ends, the equilibrium E_2 continues to be a real saddle but now with $\delta_{E_2} < 1$. This implies that the symmetric and asymmetric saddle periodic orbits that arise from the homoclinic curve $\mathbf{H_1}$ now do so to the right of this curve. From the point $\mathbf{DH_1}$ now, three new curves emerge to the right of $\mathbf{H_1}$: a saddle–node bifurcation curve of asymmetric periodic orbits, a symmetry-breaking bifurcation curve of the symmetric periodic orbits that arise from $\mathbf{H_1}$ and a homoclinic connection curve where the asymmetric periodic orbits (that arise from the aforementioned symmetry-breaking bifurcation) disappear. These three curves end at the point $\mathbf{D_3He}$ of the heteroclinic connection curve **He**. In the range of Fig. 5, they are indistinguishable from the curve $\mathbf{H_1}$, so we have not drawn them. However, we will represent these curves for other values of the parameters because they are no longer indistinguishable (see Fig. 9(b)). Remark that its theoretical study has not been addressed and falls outside the scope of this work.

For its part, the heteroclinic connection curve **He** also presents several degenerations. For their description, we denote the eigenvalues of the equilibrium E_1 (in the range of Fig. 5) by $\lambda_3 < 0 < \mathrm{Re}(\lambda_1) \leq \mathrm{Re}(\lambda_2)$, and consider the saddle quantity $\delta_{E_1} = \left|\frac{\mathrm{Re}(\lambda_1)}{\lambda_3}\right|$ where

$$\lambda_3 = a_3 = -0.05 < 0, \qquad \lambda_{2,1} = \frac{a_2 \pm \sqrt{(a_2)^2 + 4a_1}}{2}.$$

When the curve **He** emerges from **HS**, E_1 is a saddle-focus with $\delta_{E_1} < 1$ and E_2 is a real saddle with $\delta_{E_2} > 1$. The first degeneration, $\mathbf{D_1He}$, occurs at the point $(a_1, a_2) \approx (-0.04691, 0.0018)$ when $\delta_{E_2} = 1$. Since the curve **He** intersects the line $a_2 = 20a_1 + 0.94$ two times, a second degeneracy $\mathbf{D_1He}$ appears at $(a_1, a_2) \approx (-0.026603, 0.407940)$ (again, from this point, $\delta_{E_2} > 1$).

The curve **He** also undergoes some degeneracies related to the equilibrium E_1. The first one, $\mathbf{D_2He}$, occurs at the point $(a_1, a_2) \approx (-0.0334661, 0.1)$, where $\delta_{E_1} = 1$ (at this moment, E_1 is a saddle-focus; for $a_3 = -0.05$, this degeneracy occurs when **He** intersects the line $a_2 = 0.1$). A new degeneracy, $\mathbf{D_3He}$, at $(a_1, a_2) \approx (-0.027249, 0.330145)$, appears when E_1 changes from saddle-focus to real saddle (with $\delta_{E_1} \approx 3.3 > 1$). Finally, at a second point $\mathbf{D_2He}$, placed at $(a_1, a_2) \approx (-0.0259189, 0.568378)$, another degeneration $\delta_{E_1} = 1$ occurs (at this moment, E_1 is a real saddle; for $a_3 = -0.05$, this degeneracy appears when **He** intersects the line $a_2 = -20a_1 + 0.05$).

In the following, we will focus on the $\mathbf{D_3He}$ degeneracy since, according to the theoretical analysis carried out in Section 2, from this point infinitely many curves of homoclinic connections $\{\mathbf{H_n}\}$ of the equilibrium E_2 arise.

To find the first curves of homoclinic connections in the theoretically predicted sequence, we have made the bifurcation diagram for $a_2 = 0.2$, which appears in Fig. 6(a). On the one hand, the diagram in Fig. 4(a) provides an approximation of the homoclinic connection $\mathbf{H_2}$ for its numerical continuation in the (a_1, a_2)-plane for $a_3 = -0.05$. To obtain an approximation to the next homoclinic connection of the sequence, $\mathbf{H_3}$, we make the bifurcation diagram of the small-amplitude asymmetric periodic orbits that arise from $\mathbf{H_2}$. As seen in Fig. 6(a), these saddle periodic orbits experience a period-doubling bifurcation **pd**, for $(a_1, Period) \approx (-0.0306397, 234.191)$, where they become repulsive. Later, they undergo a saddle–node bifurcation **sn** for $(a_1, Period) \approx (-0.0298444, 294.739)$ (see upper inset in Fig. 6(a)). The saddle periodic orbits arising from it end in the homoclinic connection $\mathbf{H_3}$, for $a_1 \approx -0.0298450$.

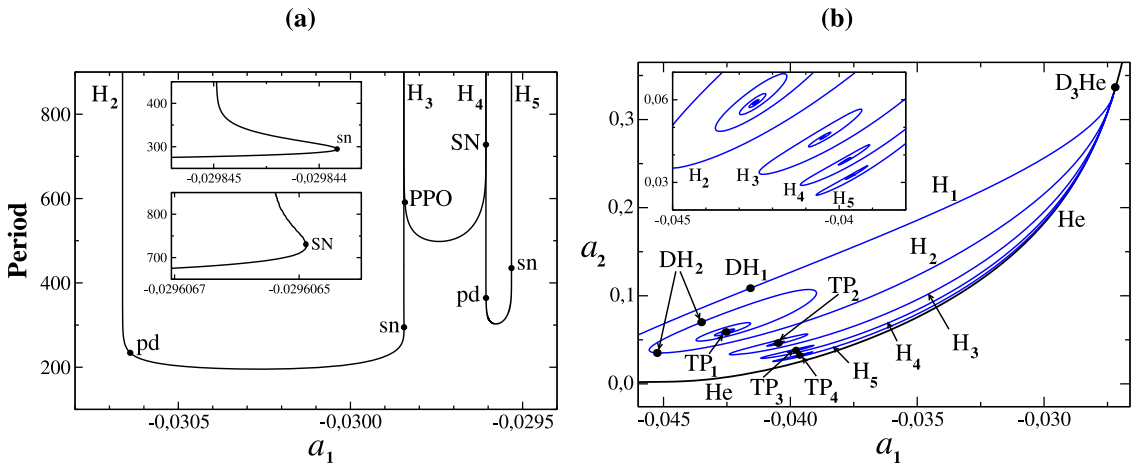

Fig. 6. For $B = 0.2$, $D = 1$, $a_3 = -0.05$: (a) Bifurcation diagram of the symmetric and asymmetric periodic orbits born in a homoclinic bifurcation $\mathbf{H_3}$ and $\mathbf{H_4}$ of E_2 for $a_2 = 0.2$. (b) Partial bifurcation set in a neighborhood of the point $\mathbf{D_3He}$.

To obtain an approximation to the following homoclinic connection $\mathbf{H_4}$, we proceed as follows. If we continue the large-amplitude saddle symmetric periodic orbit that arises from $\mathbf{H_3}$, we find that it undergoes a symmetry-breaking bifurcation **PPO**, for $(a_1, Period) \approx (-0.0298419, 591.678)$, from which it becomes repulsive. Next, it undergoes a saddle–node bifurcation **SN** for $(a_1, Period) \approx (-0.02960649, 727.905)$ (see lower inset in Fig. 6(a)). The saddle periodic orbit arising from it ends in the homoclinic connection $\mathbf{H_4}$, when $a_1 \approx -0.02960655$. Finally, with respect to $\mathbf{H_5}$, we observe that pair of small-amplitude saddle asymmetric periodic orbits which arises from $\mathbf{H_4}$ experiences two bifurcations. First, a period-doubling **pd** when $(a_1, Period) \approx (-0.0296062, 364.303)$ where the orbits become unstable and subsequently a saddle–node bifurcation **sn**, for $(a_1, Period) \approx (-0.02953227, 435.069)$. The saddle periodic orbits arising from it end in the homoclinic connection $\mathbf{H_5}$, which occurs when $a_1 \approx -0.02953228$.

In Fig. 6(b), which completes Fig. 5, the first five curves of the sequence are represented. The first of them corresponds to the curve $\mathbf{H_1}$, which ends at the Bogdanov–Takens point $\mathbf{BT^2}$. On the curve $\mathbf{H_2}$ there are two points $\mathbf{DH_2}$, placed at $(a_1, a_2) \approx (-0.0452439, 0.0351232)$ and $(a_1, a_2) \approx (-0.0434984, 0.0700326)$, where $\delta_{E_2} = 1$. In the part of the curve $\mathbf{H_2}$ that exists between both points $\mathbf{DH_2}$ it is verified that $\delta_{E_2} > 1$, while $\delta_{E_2} < 1$ at the rest of the points on the curve $\mathbf{H_2}$. Moreover, $\delta_{E_2} < 1$ at all points on the curves $\mathbf{H_3}$, $\mathbf{H_4}$ and $\mathbf{H_5}$.

Now we will examine the shape of the corresponding homoclinic orbits. To do this, we set $a_2 = 0.25$, so that we are close enough to the point $\mathbf{D_3He}$. In Fig. 7 we show the projection onto the (x, z)-plane of the one-dimensional stable manifold of E_2 for each of these five homoclinic orbits. We observe that, after *surrounding* the equilibrium E_3, as n increases, the orbit turns one more time around the z-axis and it gets closer and closer to the equilibrium E_1, which is part of the heteroclinic cycle **He**.

Indeed, in Fig. 7(a), it is observed how the projection of the orbit $\mathbf{H_1}$ (black color) surrounds the equilibrium point E_3 and subsequently approaches the z-axis, on the right side, to return to equilibrium E_2.

The projection of the homoclinic orbit $\mathbf{H_2}$ (red), after surrounding E_3, crosses the z-axis once and approaches E_2 to the left of the z-axis (see Fig. 7(b)). For its part, the projection of the homoclinic orbit $\mathbf{H_3}$ (green) crosses the z-axis twice and approaches E_2 to the right of the z-axis.

In Fig. 7(c), we observe that the projection of the homoclinic orbit $\mathbf{H_4}$ (maroon) crosses the z-axis three times and approaches E_2 to the left of the z-axis. Finally, in Fig. 7(d), we can see how the projection of the homoclinic orbit $\mathbf{H_5}$ (magenta) crosses the z-axis four times and approaches E_2 to the right of the z-axis.

We saw in Fig. 5 that the homoclinic curve $\mathbf{H_1}$ exists between the points $\mathbf{D_3He}$ and $\mathbf{BT^2}$. Now, in Fig. 6(b), we can determine where the other curves $\mathbf{H_2}$, $\mathbf{H_3}$, $\mathbf{H_4}$, and $\mathbf{H_5}$ end. Thus, the curve $\mathbf{H_2}$ finishes at the point $\mathbf{TP_1}$, placed at $(a_1, a_2) \approx (-0.0425252, 0.0589024)$ where a codimension-two heteroclinic loop between the real saddle equilibrium E_2 and the saddle-focus E_3 (and E_4) exists (a pair of heteroclinic loops appears due to the symmetry exhibited by the system (8)). This loop is called T-point heteroclinic cycle and, by abuse of notation, it is also simply named T-point (see [58–61,63]). Note that, in the case of three-dimensional systems having at least two equilibria, a T-point occurs when the one-dimensional unstable manifold of one of the equilibria and the one-dimensional stable manifold of the other equilibrium match and, simultaneously, the two-dimensional manifolds of these equilibria have a transversal intersection giving rise to a heteroclinic loop (see Fig. 8(a)). As this loop is the *easiest* one that connects the equilibria E_2 and E_4, it is called principal T-point. Although we have not drawn them because they are outside the scope of this work, it is well-known that two other curves of global connections emerge from the point $\mathbf{TP_1}$ involving the saddle-focus equilibria $E_{3,4}$: one of homoclinic orbits of E_3 (and E_4) and the other of heteroclinic orbits that connect E_3 and E_4 [59].

Note that, in $\mathbf{TP_1}$, the one-dimensional manifold of E_2 maintains the same feature as the homoclinic orbit $\mathbf{H_2}$ of Fig. 7(b) (red), namely, its projection intersects the z-axis once. Analogously, the two-dimensional manifold of E_2, arises to the left of the z-axis as occurs in $\mathbf{H_2}$ (see Figs. 7(a)–(b)).

The curves $\mathbf{H_3}$, $\mathbf{H_4}$, and $\mathbf{H_5}$ end, respectively, at the points $\mathbf{TP_2}$, $\mathbf{TP_3}$, and $\mathbf{TP_4}$, which are placed at $(a_1, a_2) \approx (-0.0404768, 0.0463592)$, $(a_1, a_2) \approx (-0.0397742, 0.0381492)$, and $(a_1, a_2) \approx (-0.0396270, 0.0323457)$. A T-point heteroclinic cycle exists at each of these points in the parameter plane. They are usually called secondary T-points because their shape is more complicated than that of the principal T-point. The projections of these heteroclinic loops onto the (x, z)-plane are drawn in Figs. 8(a)–(d). We note that the properties previously discussed about the projections of the homoclinic orbits $\mathbf{H_3}$, $\mathbf{H_4}$ and $\mathbf{H_5}$ onto the (x, z)-plane (number of times that the one-dimensional manifold of E_2 *cuts* to the z-axis and the direction of exit of its two-dimensional manifold) are also maintained in the projections of the respective heteroclinic cycles $\mathbf{TP_2}$, $\mathbf{TP_3}$ and $\mathbf{TP_4}$ (see Figs. 8(b), 8(c) and 8(d), respectively). The coexistence of multiple T-points has also been observed in several systems (see [2]).

3.2. *Increasing* a_3

As commented above, in Fig. 5 we have not drawn three bifurcation curves related to the degeneracy $\mathbf{D_3He}$ because there (for $a_3 = -0.05$) they were indistinguishable from the homoclinic curve $\mathbf{H_1}$. However,

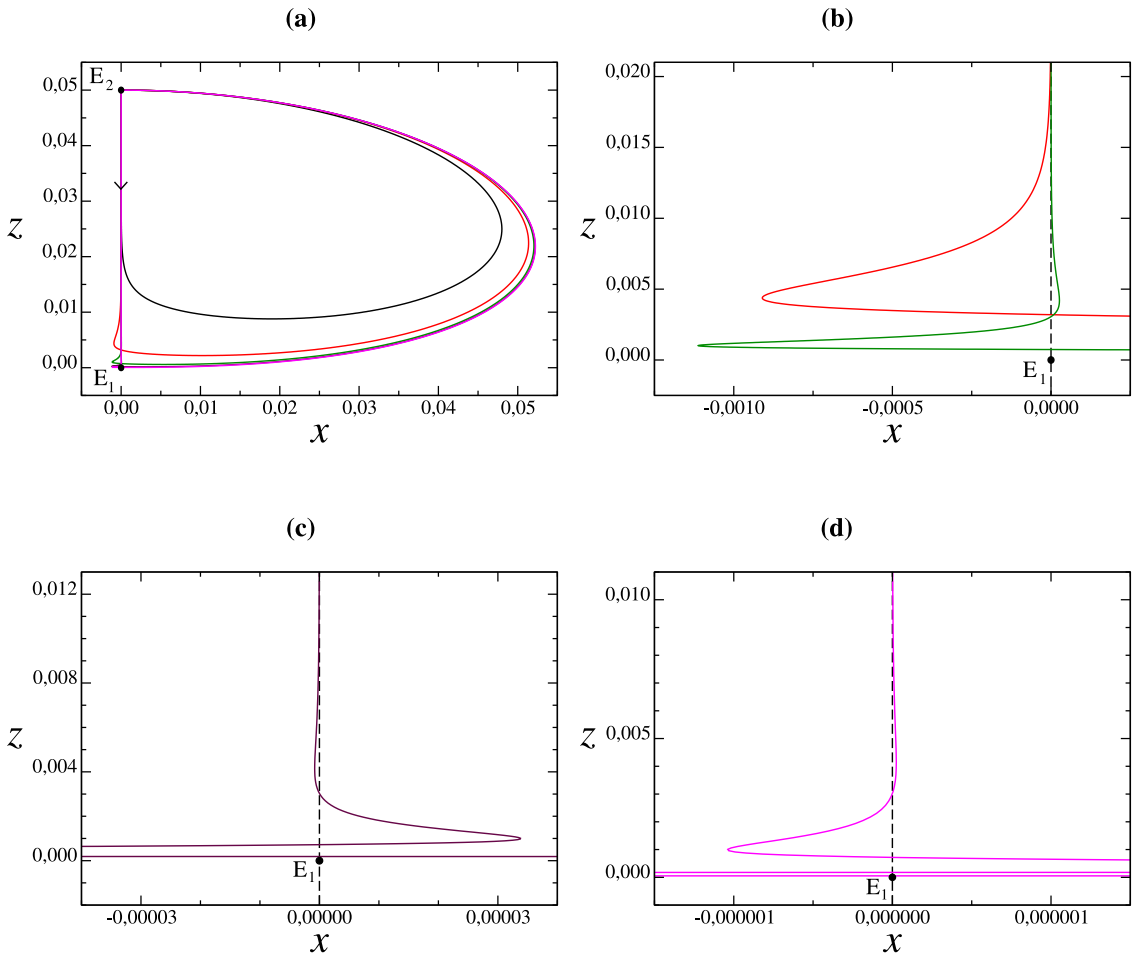

Fig. 7. For $B = 0.2$, $D = 1$, $a_2 = 0.25$, $a_3 = -0.05$, projection onto the (x, z)-plane of: (a) The homoclinic orbit $\mathbf{H_1}$ for $a_1 \approx -0.0303831$ (black), $\mathbf{H_2}$ for $a_1 \approx -0.0287938$ (red), $\mathbf{H_3}$ for $a_1 \approx -0.0284771$ (green), $\mathbf{H_4}$ for $a_1 \approx -0.0284038$ (maroon), $\mathbf{H_5}$ for $a_1 \approx -0.0283859$ (magenta). Note that because of the symmetry a pair of the corresponding homoclinic orbits exists. Zoom of panel (a) in a neighborhood of the origin E_1 with the homoclinic orbits: (b) $\mathbf{H_2}$ and $\mathbf{H_3}$; (c) $\mathbf{H_4}$; (d) $\mathbf{H_5}$. (For interpretation of the references to color in this figure legend, the reader is referred to the web version of this article.)

for other values of the parameters (now we fix $a_3 = -0.032$), it is possible to visualize them. First, in Fig. 9(a), for $a_2 = 0.15$, we draw a bifurcation diagram with these new bifurcations. We see that the small-amplitude asymmetric saddle periodic orbit that arises from the homoclinic connection $\mathbf{H_1}$ (which exists for $a_1 \approx -0.0227524$) undergoes a saddle–node bifurcation of periodic orbits **sn**, for $a_1 \approx -0.0227192$, and ends as a repulsive periodic orbit in a Hopf bifurcation **h** of E_3 when $a_1 \approx -0.0235647$. The large-amplitude saddle symmetric periodic orbit arising from $\mathbf{H_1}$ undergoes a symmetry-breaking bifurcation **PPO**, for $a_1 \approx -0.0225693$, from which it becomes repulsive. Next, it undergoes a saddle–node bifurcation of symmetric periodic orbits **SN**, for $a_1 \approx -0.0202902$, where a saddle periodic orbit emerges. This orbit later ends in a homoclinic connection to E_2, **HPPO**, located between $\mathbf{H_1}$ and $\mathbf{H_2}$, for $a_1 \approx -0.0225039$.

From the bifurcations detected in Fig. 9(a), we have drawn in Fig. 9(b) a partial bifurcation set for $a_3 = -0.032$. As can be seen, three curves emerge from the degeneration $\mathbf{DH_1}$ located on the curve $\mathbf{H_1}$ (dashed line): a curve of saddle–node bifurcations of periodic orbits **sn** (red color, of the small-amplitude asymmetric periodic orbits that arise from the curve $\mathbf{H_1}$), a curve of symmetry-breaking bifurcations **PPO** (green color, of the large-amplitude symmetric periodic orbits that arise from the curve $\mathbf{H_1}$) and a curve of homoclinic connections to E_2 **HPPO** (blue color, where the large-amplitude asymmetric saddle periodic orbits arising from the symmetry-breaking bifurcation **PPO** end, in an analogous manner to what was obtained in [70, Fig. 1] and [72, Fig. 12]). We remark that these three curves, located below the curve $\mathbf{H_1}$, also end at $\mathbf{D_3He}$.

Furthermore, this figure shows how a curve of saddle–node bifurcations of large-amplitude symmetric periodic orbits **SN** (magenta color; these orbits are related to the homoclinic connection $\mathbf{H_2}$) emerges from the point $\mathbf{D_3He}$. This curve ends in a cusp bifurcation of periodic orbits that exists for $(a_1, a_2) \approx (-0.000486385, 0.00439321)$, a point which is outside the range of the figure. From this cusp, a new saddle–node bifurcation curve **SN** (magenta color) arises. It ends at the point **IF**, when $(a_1, a_2) \approx (-0.0296209, 0.0242507)$, located on the homoclinic curve $\mathbf{H_2}$. At this point an inclination-flip degeneracy occurs, that is, the stable manifold of the equilibrium changes from orientable to nonorientable (Möbius band) and the eigenvalues satisfy certain conditions [47,64,65]. Since at the point **IF** the eigenvalues of E_2 are $(\lambda_1^*, \lambda_2^*, \lambda_3^*) \approx (-0.0358020, 0.0664527, 0.032)$ the inclination-flip is of type B [64] .

As already happened for $a_3 = -0.05$ (see Fig. 6(b)), the curve $\mathbf{H_2}$ ends at the principal T-point $\mathbf{TP_1}$. This means that, as the curve $\mathbf{H_2}$ spirals closer to $\mathbf{TP_1}$, the number of turns that the (projection of the) homoclinic connection $\mathbf{H_2}$ makes around the equilibrium E_4 increases. In an analogous way, although it does not appear in the figure, the homoclinic curves $\mathbf{H_3}$, $\mathbf{H_4}$, and $\mathbf{H_5}$ end, respectively, at the secondary T-points $\mathbf{TP_2}$, $\mathbf{TP_3}$, and $\mathbf{TP_4}$. On the other hand, as can be seen in the inset of Fig. 9(b), the homoclinic curves **HPPO** and $\mathbf{H_2}$ are very close.

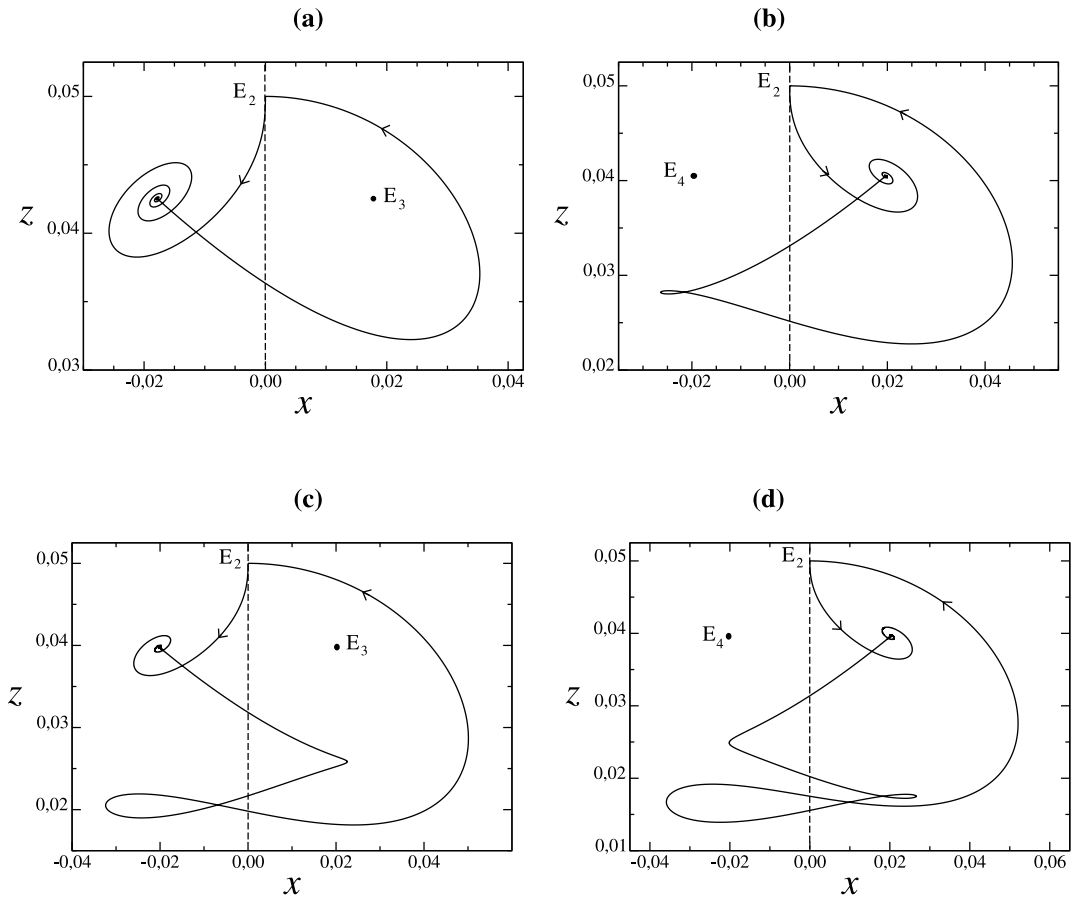

Fig. 8. For $B = 0.2$, $D = 1$, $a_3 = -0.05$, projection onto the (x, z)-plane of several T-points: (a) $\mathbf{TP_1}$, located at $(a_1, a_2) \approx (-0.0425252, 0.0589024)$. (b) $\mathbf{TP_2}$, which exists for $(a_1, a_2) \approx (-0.0404768, 0.0463592)$. (c) $\mathbf{TP_3}$, placed at $(a_1, a_2) \approx (-0.0397742, 0.0381492)$. (d) $\mathbf{TP_4}$, which occurs when $(a_1, a_2) \approx (-0.0396270, 0.0323457)$. Note that because of the symmetry a pair of the corresponding orbits exists.

In this zone, the homoclinic orbits corresponding to both curves must be very similar.

To verify this, we are going to see how the shape of the homoclinic orbits **HPPO** (blue) and $\mathbf{H_2}$ (red) evolves when we move along the corresponding curves. In the upper window of Fig. 9(c), for $a_3 = -0.032$, $a_2 = 0.15$, we represent the projection of the homoclinic orbits corresponding to the bifurcations of the diagram drawn in Fig. 9(a). We observe that the phase portrait of $\mathbf{H_2}$ is qualitatively similar to that of Fig. 7(a) corresponding to this homoclinic orbit (red). In the case of the homoclinic orbit **HPPO**, since the periodic orbit that ends in it emerges from a symmetry-breaking bifurcation, it surrounds each of the equilibria $E_{3,4}$ once. The qualitative shape of this homoclinic orbit is preserved along the entire curve **HPPO** in Fig. 9(b).

Now, when the value of the parameter a_2 decreases, the homoclinic connection curve $\mathbf{H_2}$, spirally approaches the T-point $\mathbf{TP_1}$. This means that the corresponding orbit increases the number of turns around the equilibrium E_4 before ending at E_2. This allows, as we can see in the lower window of Fig. 9(c) for $a_1 = -0.0262$, that the projections of the homoclinic orbits **HPPO** (blue; when $a_2 \approx 0.0936133$) and $\mathbf{H_2}$ (red; when $a_2 \approx 0.0901457$) are very similar and close to coinciding.

In what follows, we want to investigate how these curves interact when the value of a_3 is slightly increased. Indeed, when $a_3 = -0.03$ (see Fig. 9(d)) although both bifurcation curves continue to emerge from the point $\mathbf{D_3He}$, however, they have exchanged their endpoints, due to the contact occurred between them to an intermediate value of a_3. As a consequence, the curve **HPPO** now ends at the principal T-point $\mathbf{TP_1}$ and the curve $\mathbf{H_2}$ at the degeneracy $\mathbf{DH_1}$. A similar interaction between curves of homoclinic connections arising from a heteroclinic degeneracy $\mathbf{D_3He}$ has recently been found on another Lorenz-like system [37].

3.3. Main organizing centers

The study carried out so far of the degeneration $\mathbf{D_3He}$ in system (8) has allowed us to find other codimension-two bifurcations. Our goal now is to see how these bifurcations are organized around several codimension-three degeneracies (between them, the triple-zero bifurcation of the origin **TZ** plays a key role). This information in the (a_1, a_2, a_3)-parameter space appears in Fig. 10: we have drawn the loci where several of the codimension-two bifurcations present in Figs. 5 and 6(b) exist. Specifically, we can see the curves corresponding to the following degeneracies:

- $\mathbf{BT^1}$, Takens-Bogdanov bifurcation of the equilibrium E_1.
- $\mathbf{BT^2}$, Takens-Bogdanov bifurcation of E_2.
- **DZ**, double-zero bifurcation of E_1.
- **HZ**, Hopf-zero bifurcation of E_1.
- **HS**, Hopf–Shil'nikov heteroclinic bifurcation because the equilibrium E_1 undergoes a Hopf bifurcation.
- $\mathbf{D_1He}$, degenerate heteroclinic cycle between E_1 and E_2 because $\delta_{E_2} = 1$, being E_1 a saddle-focus and E_2 a real saddle.
- $\mathbf{D_2He}$, degenerate heteroclinic cycle between E_1 and E_2 because $\delta_{E_1} = 1$, being E_1 a saddle-focus and E_2 a real saddle.
- $\mathbf{D_3He}$, degenerate heteroclinic cycle between E_1 and E_2 because the origin E_1 changes from real saddle to saddle-focus, being E_2 a real saddle.
- $\mathbf{DH_n}$ ($n = 1, \ldots, 5$), degenerate homoclinic connections to E_2 because $\delta_{E_2} = 1$ for this real saddle ($n = 1$ blue, $n = 2$ red, $n = 3$ green, $n = 4$ maroon, $n = 5$ magenta).

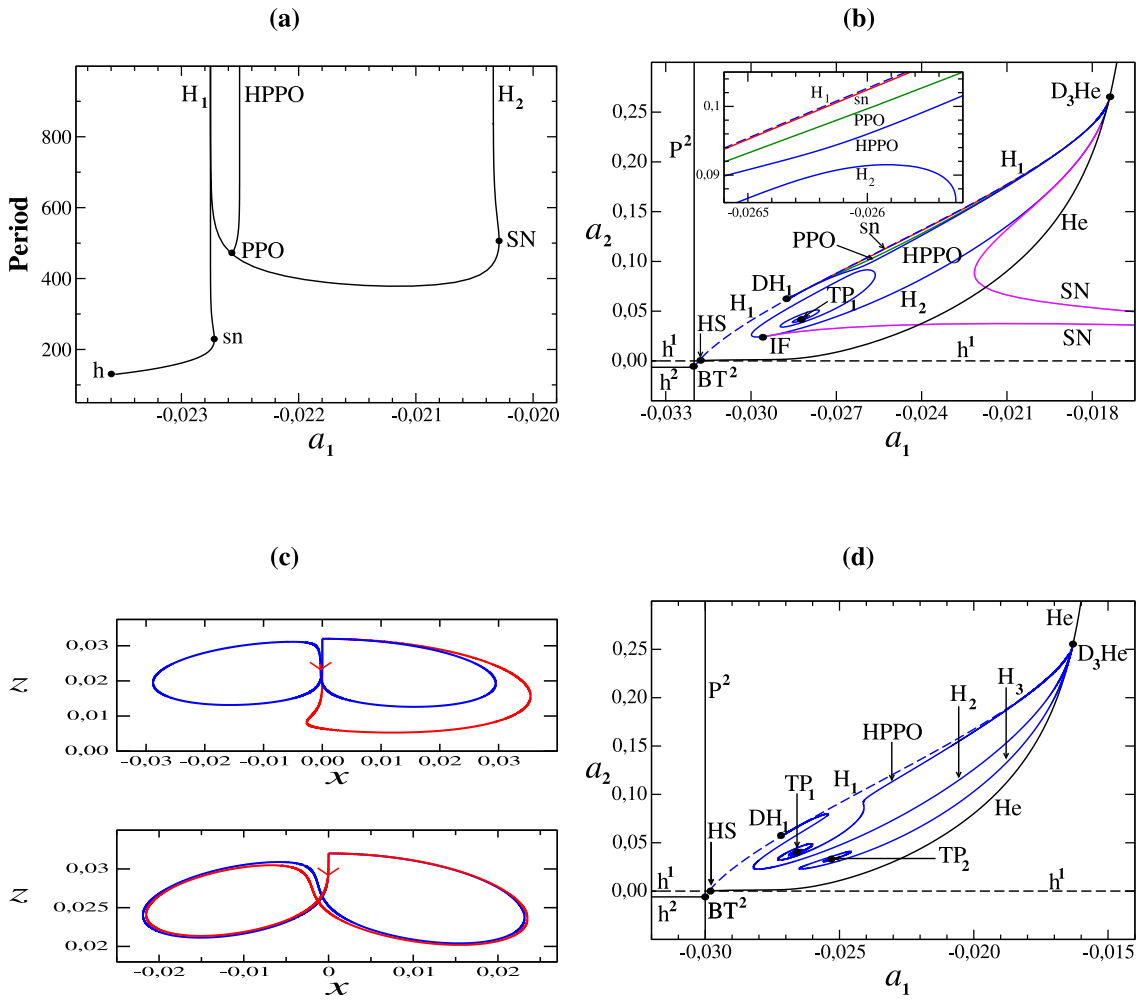

Fig. 9. For $B = 0.2, D = 1$: (a) Bifurcation diagram of the periodic orbits related to $\mathbf{H_1}$ and **PPO**, for $a_2 = 0.15$, $a_3 = -0.032$. (b) Partial bifurcation set in a neighborhood of the points $\mathbf{D_3He}$ and $\mathbf{DH_1}$, when $a_3 = -0.032$. (c) For $a_3 = -0.032$, projection onto the (x, z)-plane of the homoclinic connections **HPPO** (blue color) and $\mathbf{H_2}$ (red color) to the equilibrium E_2. The upper window corresponds to $a_2 = 0.15$ (bifurcations shown in panel (a)) whereas the lower window is obtained for $a_1 = -0.0262$ (when the corresponding curves are very close, as can be seen in the inside of panel (b)). (d) Partial bifurcation set in a neighborhood of the points $\mathbf{D_3He}$ and $\mathbf{DH_1}$, when $a_3 = -0.03$. (For interpretation of the references to color in this figure legend, the reader is referred to the web version of this article.)

- $\mathbf{TP_1}$ (red), $\mathbf{TP_2}$ (green), $\mathbf{TP_3}$ (maroon) and $\mathbf{TP_4}$ (magenta), T-point heteroclinic loops connecting E_2 and $E_{3,4}$.

As seen in Figs. 10(a)–(d), the curves $\mathbf{BT^1}$, $\mathbf{BT^2}$, **HZ**, **DZ**, **HS**, $\mathbf{D_1He}$, $\mathbf{D_2He}$, $\mathbf{D_3He}$, $\mathbf{DH_1}$, $\mathbf{TP_1}$, $\mathbf{TP_2}$, $\mathbf{TP_3}$, and $\mathbf{TP_4}$ arise from the point **TZ**, where E_1 exhibits a triple-zero bifurcation (triple-zero eigenvalue with geometrical multiplicity two). In particular, the curve $\mathbf{DH_1}$ ends at the point $\mathbf{DD_3He}$ on the curve $\mathbf{D_3He}$, for $(a_1, a_2, a_3) \approx (-0.0354111, 0.376357, -0.0648810)$, where the heteroclinic cycle experiences a double degeneration since E_1 changes from real saddle to saddle-focus and, simultaneously, $\delta_{E_2} = 1$. The existence of this degeneration $\mathbf{DD_3He}$ implies that, on the curve $\mathbf{D_3He}$, $\delta_{E_2} < 1$ in the portion between the points **TZ** and $\mathbf{DD_3He}$ and $\delta_{E_2} > 1$ in the remaining points of that curve. With respect to the curve $\mathbf{D_1He}$, it exists on both sides of the point $\mathbf{DD_3He}$ (in Fig. 10(c) we have not drawn its projection to the right of $\mathbf{DD_3He}$ since it is almost indistinguishable from the curve $\mathbf{D_3He}$). For its part, the curve $\mathbf{D_2He}$ ends at the point $(a_1, a_2, a_3) \approx (-0.305722, 1.105842, -0.552921)$, located on the curve $\mathbf{D_3He}$ (not drawn as it is outside the range of values in Figs. 10(a)–(d)). A double degeneration occurs at this new codimension-three bifurcation since the equilibrium E_1 goes from real saddle to saddle-focus and at the same time $\delta_{E1} = 1$ (because $a_3 = \lambda_3 = -\lambda_1 = -\lambda_2$), with E_2 being a real saddle.

We would like to remark three results previously found in the literature which are related to some of the bifurcations present in Fig. 10. First, the relationship of the curves $\mathbf{D_3He}$ and $\mathbf{DH_1}$ with **TZ** was already found in the system (8), for $A = -1$, $B = -0.1$, $C = 1$, and $D = 0.01$ [35, Fig. 10]. Second, the degeneracy $\mathbf{DD_3He}$ has also been detected in a Lorenz-like system [37, Fig. 7]. Third, in the Lorenz system, there is a curve of degenerate homoclinic connections of the origin analogous to the curve $\mathbf{DH_1}$ which connects the triple-zero degeneracy of the origin **TZ** with the point $(\rho, b, \sigma) = (-3, -2, -1)$ [28, Fig. 12]. At this last point, a different codimension-three degeneration is experienced since the eigenvalues at the origin are $\lambda_1 = -\lambda_2 = -\lambda_3 = -2$ (resonant eigenvalues and double real eigenvalue).

The curve $\mathbf{DH_2}$, where the homoclinic connection $\mathbf{H_2}$ experiences the degeneracy $\delta_{E_2} = 1$, also arises from the point $\mathbf{DD_3He}$. This curve ends in a spiral shape at the point $\mathbf{DTP_1}$, located at $(a_1, a_2, a_3) \approx (-0.0703837, 0.0862917, -0.0869629)$. This T-point is degenerate because $\delta_{E_2} = 1$, since the eigenvalues associated with E_2 are $\lambda_1^* = -\lambda_3^* = a_3$, $\lambda_2^* \approx 0.190647$. Analogously, the curves $\mathbf{DH_3}$, $\mathbf{DH_4}$, and $\mathbf{DH_5}$ (where the corresponding homoclinic connections $\mathbf{H_3}$, $\mathbf{H_4}$, and $\mathbf{H_5}$ are degenerate because $\delta_{E_2} = 1$) also arise from the point $\mathbf{DD_3He}$. These three curves end in a spiral shape, respectively, at the points $\mathbf{DTP_2}$, $\mathbf{DTP_3}$, and $\mathbf{DTP_4}$ (which correspond to degenerate secondary T-points that appear on the curves $\mathbf{TP_2}$, $\mathbf{TP_3}$, and $\mathbf{TP_4}$ because $\delta_{E_2} = 1$). These three points are located, respectively, at $(a_1, a_2, a_3) \approx (-0.102467, 0.0823768, -0.135772)$, $(a_1, a_2, a_3) \approx (-0.112392, 0.0670234, -0.149035)$ and $(a_1, a_2, a_3) \approx (-0.116134, 0.0551694, -0.152423)$. Due to this numerical evidence, we

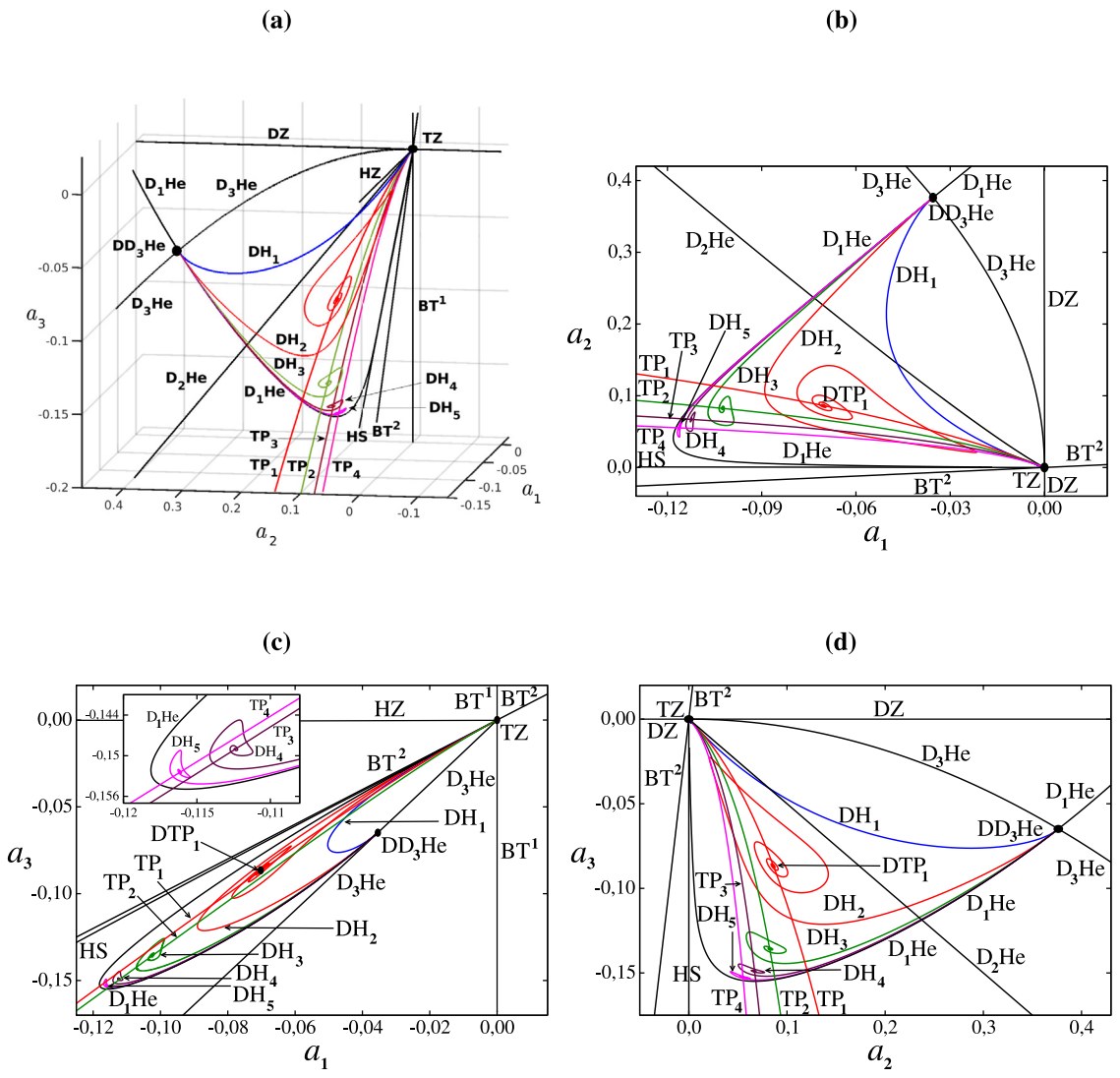

Fig. 10. For $B = 0.2, D = 1$, partial bifurcation set in the vicinity of the triple-zero bifurcation of the origin **TZ**. We represent the curves $\mathbf{BT^1}$ and $\mathbf{BT^2}$ (Takens-Bogdanov bifurcations of E_1 and E_2, respectively), **DZ** and **HZ** (double-zero and Hopf-zero bifurcations of E_1, respectively), **HS** (Hopf–Shil'nikov heteroclinic bifurcation), $\mathbf{D_1He}$ (degeneracy on **He** because $\delta_{E_2} = 1$, being E_1 a saddle-focus and E_2 a real saddle), $\mathbf{D_2He}$ (degeneracy on **He** because $\delta_{E_1} = 1$, being E_1 a saddle-focus and E_2 a real saddle), $\mathbf{D_3He}$ (degeneracy on the curve **He** when E_1 changes from real saddle to saddle-focus, being E_2 a real saddle), $\mathbf{DH_n}$, $n = 1, \dots, 5$ (degeneracy $\delta_{E_2} = 1$ on the homoclinic connection $\mathbf{H_n}$ of the equilibrium E_2; $n = 1$ blue, $n = 2$ red, $n = 3$ green, $n = 4$ maroon, $n = 5$ magenta) and $\mathbf{TP_n}$, $n = 1, \dots, 4$ (T-points where the homoclinic curves $\mathbf{H_{n+1}}$ end spiraling; $n = 1$ red, $n = 2$ green, $n = 3$ maroon, $n = 4$ magenta). The codimension-three degeneracies $\mathbf{DD_3He}$, $\mathbf{DTP_1}$, $\mathbf{DTP_2}$, $\mathbf{DTP_3}$ and $\mathbf{DTP_4}$ can also be observed. (a) In the (a_1, a_2, a_3)-parameter space. (b) Projection on the (a_1, a_2)-plane. (c) Projection on the (a_1, a_3)-plane. (d) Projection on the (a_2, a_3)-plane. In panel (b), we have not included **HZ** since it is almost indistinguishable from **HS**. In panel (d), $\mathbf{BT^1}$ is not drawn since, for $a_3 < 0$, it is almost identical to **HS**. (For interpretation of the references to color in this figure legend, the reader is referred to the web version of this article.)

conjecture that an infinite succession of curves $\{\mathbf{DH_n}\}$ arises from the point $\mathbf{DD_3He}$ which, in turn, end at the points of a sequence $\{\mathbf{DTP_n}\}$ where degenerate T-points exist (since $\delta_{E_2} = 1$).

To illustrate the complex dynamics that exist in this region of the parameter space, we draw two chaotic repellors in Figs. 11(a) and 11(b). The first corresponds to $(a_1, a_2, a_3) = (-0.115, 0.068, -0.151)$, with initial conditions $(x_0, y_0, z_0) = (10^{-20}, 0, 10^{-20})$ (close to equilibrium E_1) while the second exists when $(a_1, a_2, a_3) = (-0.0395, 0.033, -0.05)$, with initial conditions $(x_0, y_0, z_0) = (10^{-20}, 0, 0.05)$ (close to equilibrium E_2).

Since system (7), if $AC \neq 0$, is invariant, for instance, to the changes

$$(x, y, z, t, a_1, a_2, a_3, A, B, C, D) \longrightarrow (-x, y, -z, -t, a_1, -a_2, -a_3, -A, B, C, D),$$
$$(x, y, z, t, a_1, a_2, a_3, A, B, C, D) \longrightarrow (-x, y, z, -t, a_1, -a_2, -a_3, A, -B, -C, -D),$$

it is trivial to find the corresponding parameter values for which chaotic attractors exist.

4. Conclusions and future works

In this paper, we have studied a theoretical model of a degenerate heteroclinic cycle between two equilibria, which occurs when one of the involved equilibria changes from real saddle to saddle-focus (Belyakov transition). In this heteroclinic cycle, one of the heteroclinic orbits always exists (codimension-zero). We demonstrate the existence of infinitely many curves of homoclinic connections to the equilibrium, which does not exhibit the Belyakov transition. As far as we know, the analysis of this degeneration has not been previously considered in the literature. The subsequent numerical study of the Lorenz-like system (8) has allowed us to find some of the main organizing centers of its complex dynamics (see Fig. 10). In this very intricate bifurcation scenario, several codimension-three bifurcations play a remarkable role (the most important is a triple-zero bifurcation, but also doubly-degenerate heteroclinic cycles and degenerate T-points appear).

As it is known, in the unfolding of the Belyakov transition for a homoclinic connection, there are not only infinitely many homoclinic

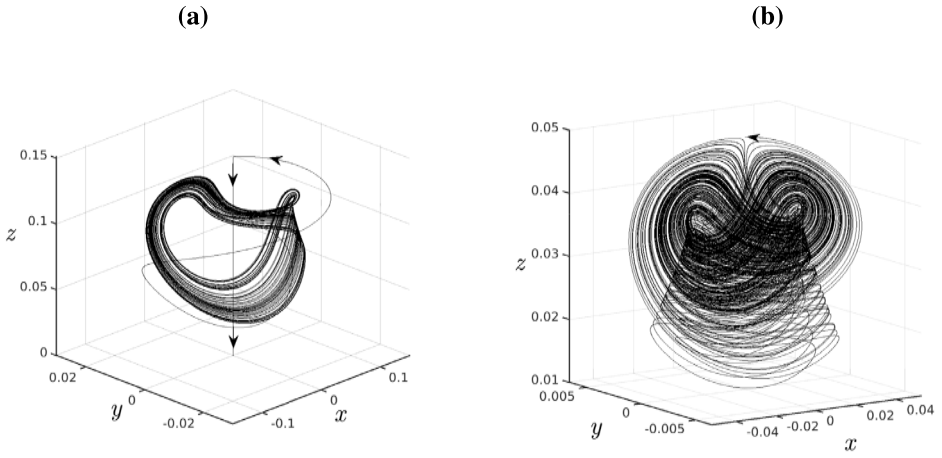

Fig. 11. For $B = 0.2$, $D = 1$, chaotic repellors present when: (a) $(a_1, a_2, a_3) = (-0.115, 0.068, -0.151)$, with initial conditions $(x_0, y_0, z_0) = (10^{-20}, 0, 10^{-20})$, integrating backwards until $t = -4000$. (b) $(a_1, a_2, a_3) = (-0.0395, 0.033, -0.05)$, with initial conditions $(x_0, y_0, z_0) = (10^{-20}, 0, 0.05)$, integrating backwards until $t = -30000$.

curves but also infinitely many saddle–node and period-doubling bifurcation curves. We remark that, although it is outside the scope of this work, a similar situation occurs in the Belyakov-like transition with a heteroclinic cycle we have studied in this paper. In the future, we intend to analyze this situation both theoretically and numerically. Due to the symmetry exhibited by system (8), we also conjecture the existence of infinitely many symmetry-breaking bifurcation curves.

A second interesting open problem that should be addressed in the future is the theoretical study of the codimension-three point $\mathbf{DD_3He}$, where the heteroclinic cycle experiences a double degeneration since, simultaneously, E_1 changes from real saddle to saddle-focus and $\delta_{E_2} = 1$. The numerical results we have obtained suggest that, from this point, infinitely many degenerate homoclinic curves $\mathbf{DH_n}$ emerge. Likewise, it seems that infinitely many surfaces of saddle–node bifurcations **sn**, symmetry-breaking bifurcations **PPO** and homoclinic connections **HPPO** also reach it. The results obtained could also help to complete the intricate bifurcation scenario that exists around a triple-zero bifurcation.

Funding sources

This work has been partially supported by the Ministerio de Economía *y* Competitividad (MTM2017-87915-C2-1-P), by the Ministerio de Ciencia, Innovación *y* Universidades (PGC2018-096265-B-I00, PID2021-123200NB-I00) and by the Consejería de Economía, Innovación, Ciencia y Empleo de la Junta de Andalucía (projects FQM-276, TIC-0130, P20_01160 and UHU-1260150).

CRediT authorship contribution statement

A. Algaba: Writing – review & editing, Writing – original draft, Methodology, Investigation, Formal analysis, Conceptualization. **F. Fernández-Sánchez:** Writing – review & editing, Writing – original draft, Methodology, Investigation, Formal analysis, Conceptualization. **M. Merino:** Writing – review & editing, Writing – original draft, Methodology, Investigation, Formal analysis, Conceptualization. **A.J. Rodríguez-Luis:** Writing – review & editing, Writing – original draft, Methodology, Investigation, Formal analysis, Conceptualization.

Declaration of competing interest

The authors declare that they have no known competing financial interests or personal relationships that could have appeared to influence the work reported in this paper.

Data availability

Data will be made available on request.

Acknowledgments

We thank the reviewers for their careful reading of the manuscript and their very constructive remarks, which have helped a lot to improve the presentation of the results.

References

[1] Lorenz EN. Deterministic non-periodic flows. J Atmos Sci 1963;20:130–41.
[2] Barrio R, Shilnikov AL, Shilnikov LP. Kneadings, symbolic dynamics and painting Lorenz chaos. Int J Bifurcation Chaos 2012;22:1230016.
[3] Pelino V, Maimone F, Pasini A. Energy cycle for the Lorenz attractor. Chaos Solitons Fractals 2014;64:67–77.
[4] Munmuangsaen B, Srisuchinwong B. A hidden chaotic attractor in the classical Lorenz system. Chaos Solitons Fractals 2018;107:61–6.
[5] Doedel EJ, Krauskopf B, Osinga HM. Global invariant manifolds in the transition to preturbulence in the Lorenz system. Indag Math 2011;22:222–40.
[6] Llibre J, Messias M, da Silva PR. Global dynamics of the Lorenz system with invariant algebraic surfaces. Int J Bifurcation Chaos 2010;20:3137–55.
[7] Algaba A, Gamero E, Merino M, Rodríguez-Luis AJ. Resonances of periodic orbits in the Lorenz system. Nonlinear Dynam 2016;84:2111–36.
[8] Algaba A, Merino M, Rodríguez-Luis AJ. Superluminal periodic orbits in the Lorenz system. Commun Nonlinear Sci Numer Simul 2016;39:220–32.
[9] Rössler OE. An equation for continuous chaos. Phys Lett A 1976;57:397–8.
[10] Algaba A, Freire E, Gamero E, Rodríguez-Luis AJ. Resonances of periodic orbits in Rössler system in presence of a triple-zero bifurcation. Int J Bifurcation Chaos 2007;17:1997–2008.
[11] Barrio R, Blesa F, Dena A, Serrano S. Qualitative and numerical analysis of the Rössler model: Bifurcations of equilibria. Comput Math Appl 2011;62:4140–50.
[12] Pivka L, Wu CW, Huang A. Lorenz equation and Chua's equation. Int J Bifurcation Chaos 1996;6:2443–89.
[13] Rocha R, Medrano-T RO. Stability analysis of the Chua's circuit with generic odd nonlinearity. Chaos Solitons Fractals 2023;176:114112.
[14] Xing T, Pusuluri K, Shilnikov AL. Ordered intricacy of Shilnikov saddle-focus homoclinics in symmetric systems. Chaos 2021;31:073143.
[15] Algaba A, Merino M, Rodríguez-Luis AJ. Homoclinic connections near a Belyakov point in Chua's equation. Int J Bifurcation Chaos 2005;15:1239–52.
[16] Algaba A, Merino M, Rodríguez-Luis AJ. Homoclinic interactions near a triple-zero degeneracy in Chua's equation. Int J Bifurcation Chaos 2012;22:1250129.
[17] Algaba A, Fernández-Sánchez F, Merino M, Rodríguez-Luis AJ. Analysis of the T-point-Hopf bifurcation with $\mathbb{Z}_2$-symmetry. Application to Chua's equation. Int J Bifurcation Chaos 2010;20:979–93.
[18] Freire E, Rodríguez-Luis AJ, Gamero E, Ponce E. A case study for homoclinic chaos in an autonomous electronic circuit. A trip from Takens–Bogdanov to Hopf–Sil'nikov. Physica D 1993;62:230–53.
[19] Algaba A, Gamero E, Rodríguez-Luis AJ. A bifurcation analysis of a simple electronic circuit. Commun Nonlinear Sci Numer Simul 2005;10:169–78.

[20] Faradja P, Qi G. Analysis of multistability, hidden chaos and transient chaos in brushless DC motor. Chaos Solitons Fractals 2020;132:109606.
[21] Kazakov A. On bifurcations of Lorenz attractors in the Lyubimov–Zaks model. Chaos 2021;31:093118.
[22] Algaba A, Merino M, Qin BW, Rodríguez-Luis AJ. Study of a dynamical system with a strange attractor and invariant tori. Phys Lett A 2019;383:1441–9.
[23] Guckenheimer J, Holmes PJ. Nonlinear oscillations, dynamical systems, and bifurcations of vector fields. New York: Springer; 1983.
[24] Chow S, Li C, Wang D. Normal forms and bifurcation of planar vector fields. Cambridge: Cambridge University Press; 1994.
[25] Wiggins S. Introduction to applied nonlinear dynamical systems and chaos. Springer: New York; 2003.
[26] Kuznetsov YA. Elements of applied bifurcation theory. New York: Springer; 2004.
[27] Algaba A, Domínguez-Moreno MC, Merino M, Rodríguez-Luis AJ. Study of the Hopf bifurcation in the Lorenz, Chen and Lü systems. Nonlinear Dynam 2015;79:885–902.
[28] Algaba A, Domínguez-Moreno MC, Merino M, Rodríguez-Luis AJ. Takens-Bogdanov bifurcations of equilibria and periodic orbits in the Lorenz system. Commun Nonlinear Sci Numer Simul 2016;30:328–43.
[29] Belykh VN, Bykov VV. Bifurcations for heteroclinic orbits of a periodic motion and a saddle-focus and dynamical chaos. Chaos Solitons Fractals 1998;9:1–18.
[30] Algaba A, Freire E, Gamero E, Rodríguez-Luis AJ. Analysis of Hopf and Takens–Bogdanov bifurcations in a modified van der Pol–Duffing oscillator. Nonlinear Dynam 1998;16:369–404.
[31] Gazor M, Sadri N. Bifurcation controller designs for the generalized cusp plants of Bogdanov–Takens singularity with an application to ship control. SIAM J Control Optim 2019;57:2122–51.
[32] Lv Y, Pei Y, Wang Y. Bifurcations and simulations of two predator–prey models with nonlinear harvesting. Chaos Solitons Fractals 2019;120:158–70.
[33] Chan-López E, Castellanos V. Biological control in a simple ecological model via subcritical Hopf and Bogdanov–Takens bifurcations. Chaos Solitons Fractals 2022;157:111921.
[34] Saha P, Mondal B, Ghosh U. Dynamical behaviors of an epidemic model with partial immunity having nonlinear incidence and saturated treatment in deterministic and stochastic environments. Chaos Solitons Fractals 2023;174:113775.
[35] Algaba A, Domínguez-Moreno MC, Merino M, Rodríguez-Luis AJ. Double-zero degeneracy and heteroclinic cycles in a perturbation of the Lorenz system. Commun Nonlinear Sci Numer Simul 2022;111:106482.
[36] Maurício de Carvalho JPS, Rodrigues AA. SIR model with vaccination: bifurcation analysis. Qual Theory Dyn Syst 2023;22:105.
[37] Algaba A, Domínguez-Moreno MC, Merino M, Rodríguez-Luis AJ. A double-zero bifurcation in a Lorenz-like system. Nonlinear Dynam 2024;112:2305–30.
[38] Dumortier F, Ibáñez S, Kokubu H, Simó C. About the unfolding of a Hopf-zero singularity. Discrete Contin Dyn Syst 2013;33:4435–71.
[39] Baldomá I, Ibáñez S, Seara TM. Hopf-zero singularities truly unfold chaos. Commun Nonlinear Sci Numer Simul 2020;84:105162.
[40] Vladimirov AG, Volkov DY. Low-intensity chaotic operations of a laser with a saturable absorber. Opt Commun 1993;100:351–60.
[41] Algaba A, Freire E, Gamero E, Rodríguez-Luis AJ. A note on the triple-zero linear degeneracy: normal forms, dynamical and bifurcation behaviors of an unfolding. Int J Bifurcation Chaos 2002;12:2799–820.
[42] Drubi F, Ibáñez S, Pilarczyk P. Nilpotent singularities and chaos: Tritrophic food chains. Chaos Solitons Fractals 2021;142:110406.
[43] Gonchenko S, Kazakov A, Turaev D, Shilnikov AL. Leonid Shilnikov and mathematical theory of dynamical chaos. Chaos 2022;32:010402.
[44] Algaba A, Freire E, Gamero E, Rodríguez-Luis AJ. An exact homoclinic orbit and its connection with the Rössler system. Phys Lett A 2015;379:1114–21.
[45] Belhaq M, Houssni M, Freire E, Rodríguez-Luis AJ. Asymptotics of homoclinic bifurcation in a three-dimensional system. Nonlinear Dynam 2000;21:135–55.
[46] Champneys AR, Kuznetsov YA. Numerical detection and continuation of codimension–two homoclinic bifurcations. Int J Bifurcation Chaos 1994;4:785–822.
[47] Homburg AJ, Sandstede B. Homoclinic and heteroclinic bifurcations in vector fields. In: Broer H, et al., editors. In: Handbook of dynamical systems, vol. 3, Amsterdam: Elsevier; 2010, p. 379–524.
[48] Belyakov LA. Bifurcation set in a system with homoclinic saddle curve. Math Notes Acad Sci USSR 1980;28:910–6.
[49] Belyakov LA. Bifurcation of systems with homoclinic curve of a saddle-focus with saddle quantity zero. Math Notes Acad Sci USSR 1984;36:838–43.
[50] Barrio R, Blesa F, Serrano S, Shilnikov A. Global organization of spiral structures in biparameter space of dissipative systems with Shilnikov saddle-foci. Phys Rev E 2011;84(2011):035201.
[51] Malykh S, Bakhanova Y, Kazakov A, Pusuluri K, Shilnikov A. Homoclinic chaos in the Rössler model. Chaos 2020;30:113126.
[52] Kuznetsov YA, de Feo O, Rinaldi S. Belyakov homoclinic bifurcations in a tritrophic food chain model. SIAM J Appl Math 2001;62:462–87.
[53] Algaba A, Merino M, Rodríguez-Luis AJ. Analysis of a Belyakov homoclinic connection with $\mathbb{Z}_2$-symmetry. Nonlinear Dynam 2012;69:519–29.
[54] Bella G. Homoclinic bifurcation and the Belyakov degeneracy in a variant of the Romer model of endogenous growth. Chaos Solitons Fractals 2017;104:452–60.
[55] Hirschberg P, Knobloch E. Šil'nikov–Hopf bifurcation. Physica D 1993;62:202–16.
[56] Deng B, Sakamoto K. Šil'nikov–Hopf bifurcations. J Differential Equations 1995;119:1–23.
[57] Champneys AR, Rodríguez-Luis AJ. The nontransverse Shil'nikov–Hopf bifurcation: uncoupling of homoclinic orbits and homoclinic tangencies. Physica D 1999;128:130–58.
[58] Bykov VV. The bifurcations of separatrix contours and chaos. Physica D 1993;62:290–9.
[59] Glendinning P, Sparrow C. T-points: A codimension two heteroclinic bifurcation. J Stat Phys 1986;43:479–88.
[60] Creaser JL, Krauskopf B, Osinga HM. α-flips and T-points in the Lorenz system. Nonlinearity 2015;28:R39–65.
[61] Fernández-Sánchez F, Freire E, Rodríguez-Luis AJ. T-points in a $\mathbb{Z}_2$-symmetric electronic oscillator. (I) Analysis. Nonlinear Dynam 2002;28:53–69.
[62] Fernández-Sánchez F, Freire E, Rodríguez-Luis AJ. Analysis of the T-point-Hopf bifurcation. Physica D 2008;237:292–305.
[63] Rodrigues AAP. Repelling dynamics near a Bykov cycle. J Dynam Differential Equations 2013;25:605–25.
[64] Giraldo A, Krauskopf B, Osinga HM. Saddle invariant objects and their global manifolds in a neighborhood of a homoclinic flip bifurcation of case B. SIAM J Appl Dyn Syst 2017;16:640–86.
[65] Algaba A, Domínguez-Moreno MC, Merino M, Rodríguez-Luis AJ. Study of a simple 3D quadratic system with homoclinic flip bifurcations of inward twist case C_{in}. Commun Nonlinear Sci Numer Simul 2019;77:324–37.
[66] Golmakani A, Homburg AJ. Lorenz attractors in unfoldings of homoclinic-flip bifurcations. Dyn Syst 2011;26:61–76.
[67] Algaba A, Fernández-Sánchez F, Merino M, Rodríguez-Luis AJ. Analysis of the T-point-Hopf bifurcation in the Lorenz system. Commun Nonlinear Sci Numer Simul 2015;22:676–91.
[68] Belyakov L. The bifurcation set in a system with a homoclinic saddle curve. Mat Zametki 1981;28:910–6.
[69] Shimizu T, Morioka N. On the bifurcation of a symmetric limit cycle to an asymmetric one in a simple model. Phys Lett A 1980;76:201–4.
[70] Shil'nikov AL. On bifurcations of the Lorenz attractor in the Shimizu-Morioka model. Physica D 1993;62:338–46.
[71] Shil'nikov AL. Homoclinic phenomena in laser models. Comput Math Appl 1997;34:245–51.
[72] Rucklidge AM. Chaos in a low-order model of magnetoconvection. Physica D 1993;62:323–37.
[73] Liu C, Liu T, Liu L, Liu K. A new chaotic attractor. Chaos Solitons Fractals 2004;22:1031–8.
[74] Mello LF, Messias M, Braga DC. Bifurcation analysis of a new Lorenz-like chaotic system. Chaos Solitons Fractals 2008;37:1224–55.
[75] Gamero E. On the normal form of the triple-zero degeneracy with geometric multiplicity two. Dyn Contin Discrete Ser A 2001;8:531–50.
[76] Doedel EJ, Champneys AR, Dercole F, Fairgrieve T, Kuznetsov Y, Oldeman BE, et al. Auto07-p: Continuation and bifurcation software for ordinary differential equations (with HomCont). Technical report, Concordia University; 2010.